Detection of Breast Cancer Microcalcifications in Digitized Mammograms

Developing Segmentation and Classification Techniques for the Processing of MIAS Database Mammograms Based on the Wavelet Decomposition Transform and Support Vector Machines

Husam E. I. Al-Osta

Submitted for the Degree of
Doctor of Philosophy

Department of Electronic Imaging and Media Communications
School of Informatics
University of Bradford
2010

ABSTRACT

Keywords

Mammography, wavelet, feature extraction, support vector machines, segmentation

Mammography is used to aid early detection and diagnosis systems. It takes an x-ray image of the breast and can provide a second opinion for radiologists. The earlier detection is made, the better treatment works. Digital mammograms are dealt with by Computer Aided Diagnosis (CAD) systems that can detect and analyze abnormalities in a mammogram. The purpose of this study is to investigate how to categories cropped regions of interest (ROI) from digital mammogram images into two classes; normal and abnormal regions (which contain microcalcifications).

The work proposed in this thesis is divided into three stages to provide a concept system for classification between normal and abnormal cases. The first stage is the Segmentation Process, which applies thresholding filters to separate the abnormal objects (foreground) from the breast tissue (background). Moreover, this study has been carried out on mammogram images and mainly on cropped ROI images from different sizes that represent individual microcalcification and ROI that represent a cluster of microcalcifications. The second stage in this thesis is feature extraction. This stage makes use of the segmented ROI images to extract characteristic features that would help in identifying regions of interest. The wavelet transform has been utilized for this process as it provides a variety of features that could be examined in future studies. The third and final stage is classification, where machine learning is applied to be able to distinguish between normal ROI images and ROI images that may contain microcalcifications. The result indicated was that by combining wavelet transform and SVM we can distinguish between regions with normal breast tissue and regions that include microcalcifications.

Acknowledgment

I owe my deepest gratitude and special thanks to Dr. Rami Qahwaji as primary supervisor. His expertise, inspiration, guidance, constructive suggestions and supervision helped me finish my PhD. I also would like to express my gratitude to Dr. Stanley Ipson as second supervisor for his thoughtful ideas and support in research and work. He has assisted in numerous ways to improve my knowledge of techniques in image processing.

I am obliged to many of my colleagues who supported me during my research work and with whom I also had happy days during my hard times. I want to thank them all for their support, help, interest and valuable hints.

To my beloved wife, I would like to express my undying love and gratitude for her patient love, friendship and support enabled me to complete this work. Finally, I dedicate my thesis to my parents for their constant encouragement, love and support because none of this would have been possible without them.

Table of Content

List of Figures

viii

List of Tables

Chapter 1

Introduction

1.1. Breast Cancer and Mammography

Breast cancer is a potentially fatal disease that is growing in frequency in developed countries [1] and is becoming a major public health problem among women. Early detection of this disease can aid in decreasing the number of patients dying by 20% to 30% [2] because the earlier the detection is made, the better treatment works. Breast cancer is the result of abnormal cells that spread beyond the ducts or lobules, invading the surrounding tissue and lymph nodes or blood stream. Diagnosis can be done by several types of biopsy: fine needle aspiration cytology (with sensitivity of 90% - 95%); excision biopsy; frozen section biopsy; and by ultrasound; and mammography [3].

Using mammography is cheaper than biopsy methods and is the most reliable method for early detection of this disease. Mammography captures x-ray images of breasts which are then interpreted by radiologists to locate any abnormalities that may indicate cancerous changes. For several reasons including the different types of breast tissues, low contrast images, noise and the presence of other features, this can be a difficult job for a radiologist. Mistakes by radiologists might lead to the misinterpretation of abnormalities and result in patients dying. By providing an independent second opinion, Computer Aided Detection (CAD) or Computer Aided diagnosis (CADx) systems [4] could help radiologists in the early detection of breast cancer. These systems should be considered as supportive tools that provide

radiologists with the potential ability to detect abnormalities earlier and faster. On the other hand, it is important for future studies to distinguish between computer-aided detection and computer-aided diagnosis systems. The latter CAD system could help radiologists to classify the abnormalities as benign or malignant, which would provide specificity [5].

Usually the mammogram process starts by taking an x-ray of the breast to generate a hard copy, to be handled by a radiologist. Then the mammogram is interpreted using a magnifier to examine different areas of the breast. This is due to the nature of some tumour types that are difficult to be seen by the human eye, as they could be less than 1 mm (i.e. microcalcifications); unlike other types of tumours such as masses. Depending on the expertise of the radiologist, she/he then could make a decision of what level of risk there is and what treatment is needed. If there is still uncertainty about the case, radiologists would then go through the biopsy procedure, a procedure which might cause anxiety to the patient. Therefore, by providing a computer system that could aid radiologists in interpreting and analysing a mammogram image, providing a second opinion, this could improve the chances of detecting and diagnosing tumours. However, the final decision is made by the radiologist regarding the possibility of the presence of a cancerous tumour.

The original x-ray film is converted to a digital copy that could be read by a computer under special applications designed for this specific purpose. Since there are several types of digital mammography computer aided systems, radiologists can get assistance in different ways. There are computer aided diagnosis systems that can analyse a mammogram to give a report of what sort of tumour is detected and in what category it is classified. There are computer aided detection systems that can

help radiologists in locating any abnormal object. Or there are basic viewing and image enhancement systems that provide simple tools such as the ability to zoom in on a digital mammogram image, inverting between black and white on the image and increase/decrease the grey shades; so that a radiologist could have a clearer look of certain areas, or regions, of interest.

1.2. Importance of this Work and Technical Challenges

Digital mammogram images are grey scale images which can be used to check for various breast abnormalities. Among these the main tumour type to be studied is microcalcifications, which are the smallest tumour types within the breast, with a size less than 1mm across [6, 7]. Therefore, digital mammography is an essential process to aid radiologists in studying and diagnosing mammogram images by giving them a tool that provides aid with the freedom of selecting certain areas that the radiologist is suspicious of. This process aims to provide radiologists with a second opinion in studying a mammogram case. Moreover, some of the methods that have been adopted are improved to be able to perform their tasks in different environments or to detect different types of abnormality (i.e. from detecting masses to microcalcifications).

In order to proceed, microcalcifications and other suspicious objects need to be segmented from the background. Since it is an essential step to locate and to take out these regions for detailed analyse and not spend unnecessary time analysing the background. This needs an efficient segmentation method that can detect potential microcalcification peaks. Thus, the use of special filters has been adopted for this purpose. The main problem that remains is to distinguish between true positives (i.e. microcalcifications) and false positives (i.e. other objects than microcalcifications or

- 3 -

artefacts); as some of these artefacts share the same characteristics as microcalcifications in shape, size or pixel intensity. Further, it is crucial to keep in mind the false negative that represents microcalcifications that are not detected or considered as artefact or noise. This has to be considered by configuring the thresholding parameters to match their characteristics. Moreover, to test the detection against true positive and false positive, regions of interest are cropped prior to the segmentation stage into two sets. Each set enclosing images that contain cases with microcalcifications and images with normal breast tissue. The first set includes regions of interest that represent clusters of microcalcifications and the second set represents individual microcalcification.

It is important to find some unique features that correspond to the microcalcification characteristics. These features would be the key to distinguish such an abnormality from a normal breast tissue that contains other objects than microcalcification. These features then will be needed to classify segmented regions into two classes, normal or abnormal. It is of crucial importance to apply a classification method in such a way to be able to distinguish and obtain a high level of classification accuracy between normal breast tissue and regions that contain microcalcifications, as well as maintaining the false positive at its minimum level, since the segmentation process will help in locating microcalcifications and any suspicious objects within a cropped region of interest. Therefore, yet again a classification process is needed to distinguish between regions of interest that contain microcalcifications and those that do not.

1.3.   Aims and Objectives of the Research

The main reason for the work presented in this thesis is to assist future development of the diagnostic uses of digital mammography. This is done by creating a concept CAD system that is able to perform detection for suspicious objects within images of regions of interest and then to be able to distinguish between normal and abnormal objects detected. By investigating how such a problem could be solved, combinations of methods and algorithms are modified and improved to achieve high classification accuracy results in short times. This could potentially provide assistance to radiologists interpreting mammograms by providing a second opinion that would draw the attention of the radiologist to some areas that are missed or to confirm what the radiologist already suspected.

Therefore, to sum up the main objectives of this thesis:

- Presenting the use of different region of interest image sizes (areas show cluster of microcalcifications that depends on the cluster size and areas showing individual microcalcification); this is to be run under the same process.

- To present modified thresholding filters, to locate abnormality of microcalcifications types, that could be applied to regions of interest in images provided by radiologists or cropped from a full mammogram image.

- Proposing the use of wavelet transform for feature extraction; this is by investigating different wavelet types and number of features.

- Plan of using support vector machines to distinguish and categorise between normal and abnormal breast tissue regions.

Basically, a mammographic based diagnosis system is divided into three main stages. The first stage is the localisation of potential microcalcifications and other suspicious

objects, the second stage is feature extraction which is used to identify the information from within segmented regions and finally the classification stage will process the extracted features and offer diagnostic decisions.

In other words, to define the main problems in this study they could be summarized by the following points:

- The low contrast between calcifications and surrounding tissue. When the surrounding tissues have similar or higher intensity calcifications are difficult to detect.

- The unpredictable shape, size and location of calcifications; even when found in the same cluster, are slightly different. Breast structures such as blood vessels or milk ducts and clatter, none of which are related to abnormalities, frequently have similar characteristics to calcifications. This can result in false positive detections which may cause patients unnecessary anxiety.

- To be able to provide a proper diagnosis for a mammogram, that will aid radiologists in this task; a huge number of samples that contain a variety of abnormalities need to be trained in such systems.

1.4.   Outlines of the Thesis

The remainder of the thesis is composed of five chapters. Chapter two presents a literature review of various existing methods from the research area of digital mammography. This chapter includes three main sections which cover previous research on segmentation, feature extraction and classification.

The particular implementations of the proposed system are discussed in chapters three, four and five. Chapter three includes work on segmentation including the thresholding techniques applied and the application to different sizes of regions of

interest. Chapter four includes work on feature extraction using the discrete wavelet transform, applied to the segmented images. A set of features can represent a full image or a small region of an image. The quality of the extracted features depends on the degree to which they can accurately represent the region and discriminate between the different classes. Chapter five includes the work done using the features as input to a machine learning process to classify the normal and abnormal cases. The conclusion and suggestions for future work are presented in Chapter Six.

References:

1. Bird, R.E., Wallace, T.W., and Yankaskas, B.C., *Analysis of cancers missed at screening mammography.* Radiology, 1992. **184**(3): pp. 613-617.

2. Coakley, K., Quintarelli, F., Doorn, T.v., and Hirst, C., *Classification of Equivocal Mammograms through Digital Analysis.* The breast, 1994. **3**(4): pp. 222-226.

3. *Breast Cancer Manual*, in *Dr. Soliman Fakeeh Hospital*: Jeddah, K.S.A.

4. Yusof, N.M., Isa, N.A.M., and Sakim, H.A.M., *Computer-Aided Detection and Diagnosis for Microcalcifications in Mammogram: A Review.* International Journal of Computer Science and Network Security, 2007. **7**(6): pp. 202-208.

5. Lo, J.Y., Gavrielides, M.A., Markey, M.K., and Jesneck, J.L. *Computer-aided classification of breast microcalcification clusters: merging of features from image processing and radiologists.* in Proceedings of the SPIE on Medical Imaging 2003: Image Processing. 2003. San Diego, CA, USA.

6. Bocchi, L. and Nori, J., *Shape analysis of microcalcifications using Radon transform.* Medical Engineering and Physics, 2007. **29**(6): pp. 691-698.

7. Sheshadri, H.S. and Kandaswamy, A., *Computer Aided Diagnosis of Digital Mammograms.* Information Technology Journal, 2006. **5**(2): pp. 342-346.

Chapter 2

Literature Survey

2.1. Introduction

In this chapter, we take a closer look at how the literature survey has covered a variety of significant studies in digital mammography at different levels of image processing namely: segmentation, feature extraction and classification. Some of these studies are selected as benchmarks or include methods and algorithms that have been modified and applied in this research. Each study has obtained a certain mammographic database for different purposes. Some studies have applied their methods on more than one database while most of them utilised only one. Several studies that have been mentioned in this chapter and their methods applied to the same mammographic database that has been used in this research as well. This makes it possible to compare results from the authors' research study with other studies. Also an overview of mammogram abnormalities, presented in this chapter, investigates the characteristics described in other studies, to help this research study handle these abnormalities.

The rest of this chapter is organised as follows. A description of the MIAS mammography database used in the current work is provided in Section 2.2 with an overview of the characteristics of different types of breast abnormalities in Section 2.3. Section 2.4 surveys studies related to segmentation methods that have been applied in the mammography area. In Section 2.5 various feature extraction techniques from other studies are shown. Then machine learning and classification

studies and their results from other studies are presented in Section 2.7. Section 2.7 is a short summary.

2.2. Mammography Database

Selecting a benchmark database makes it easier to compare results obtained with those from other studies. For that reason, the images that have been used in the present work are the full size images from the Mammographic Image Analysis Society (MIAS) database [1]. This database is one of two popular mammography databases available in the field of digital mammography; the other is the Digital Database of Screening Mammography (DDSM). Moreover, there are other mammography databases available but rarely used such as the Nijmegen database and the Lawrence Livermore National Laboratories (LLNL) database.

MIAS is an organization of UK research groups interested in promoting an understanding of mammograms. The database contains left and right breast images for 161 patients. It contains different types of abnormalities including the type that this study is interested in, microcalcifications. Each individual image is accompanied by information, which includes the breast type and the abnormality type and location. The location of an abnormality is specified using three variables: the x and y coordinates of a point and the radius of a circle centred on the point. This database is very helpful as expert radiologists have manually determined centres and radii appropriate to enclose whole clusters of microcalcifications. The mammogram images are available in four sizes: small (4320 x 1600), medium (4320 x 2048), large (4320 x 2600) and extra large (4000 x 5200). The largest mammogram image comprises about 21 MB of disk space. The mammogram images are digitized with a special resolution of 50μm x 50μm and 8 bit grey depth. This database contains 320

mammogram images and a database manual provides descriptive information about the individual images. The images are divided into categories according to the type of the lesion, the severity of the abnormality, and the type of the background breast tissue.

The first category, lesion type, is divided into 7 main subcategories: Normal (NORM), Architectural distortion (ARCH), Asymmetry (ASYM), Microcalcification (CALC), Circumscribed masses (CIRC), Ill-defined masses (MISC), and Spiculated lesions (SPIC). The second category, severity of abnormality, is divided into 2 main subclasses: Benign and Malignant. The third category, background tissue, is divided into 3 main subclasses: Fatty, Fatty-glandular, and Dense-glandular. In Figure 2.2 below a sample from the MIAS manual containing seven columns of information, is shown. The first column is the name of the mammogram case image where the last two letters from the name represent either left breast 'l' or right breast 'r' and the other letter is the size of the mammogram image (i.e. large 'l', medium 'm' and small 's'). The second column is the type of the breast tissue as mentioned before (i.e. Fatty 'F', Fatty-Glandular 'G' and Dense-Glandular 'D'). The third column is the lesion type and the fourth column is the severity of abnormality. Finally, the last three columns represent the location of abnormalities using x-coordinates, y-coordinates and radius of a circle containing the abnormality.

```
mdb20911   G   CALC   M   2126 1842 758
mdb210r1   G   NORM

mdb211lm   G   CALC   M   1423 1698 350
mdb212rm   G   CALC   B

mdb213ls   G   CALC   M   2193  940 660
mdb214rs   G   CALC   B

mdb215ll   D   NORM
mdb216r1   D   CALC   M   spread

mdb217ll   G   NORM
mdb218r1   G   CALC   B   1694 1275 1325

mdb219ll   G   CALC   B   3136 1439 1161
mdb220r1   G   NORM

mdb221lm   D   NORM
mdb222rm   D   CALC   B   2502 1482 566

mdb223ls   D   CALC   B   2043  846 754
           D   CALC   B   2231 1116 484
```

Figure 2.2 MIAS manual of calcifications and normal cases

2.2.1 Analysis of the MIAS Database

A total of 25 mammogram digital images containing microcalcifications exist in the MIAS database. The MIAS manual indicates that 20 mammograms have been annotated by expert radiologists with circles surrounding clusters of microcalcifications. In addition, there are 3 mammograms that have not been marked, because the microcalcifications are distributed over most of the breast region rather than concentrated at discrete locations. There are also 2 mammogram images that have not been marked but nevertheless contain microcalcifications in unspecified areas. It is noted that, by taking region of interests (ROI) from the 20 mammograms that have been expertly marked, 25 clusters of microcalcifications are produced. While most of the mammogram images contain just one microcalcification

cluster, a few of other mammograms contain more than one cluster. The multi-cluster image cases are as follows:

- mdb223ls with 2 clusters
- mdb226rm with 3 clusters
- mdb239ll with 2 clusters
- mdb249ls with 2 clusters

Table 2.1 specifies the numbers of benign and malignant clusters and the numbers of corresponding images according to the database manual.

Table 2.1 Number of clusters and mammogram images containing microcalcifications

	Benign	Malignant	Total
Mammogram Images	10	10	20
Cluster of MCs (ROI)	13	12	25

2.2.2 The Characteristics of Breast Abnormalities

The characteristics of breast tissues can differ from woman to woman. Therefore, any abnormalities present can also show different features. Abnormalities that are detected in regions of interest (ROI) defined within the breast are divided into two main types: Benign and Malignant. Abnormalities are also divided into several types as mentioned before: ARCH, ASYM, CALC, CIRC, MISC, and SPIC. However, regarding the microcalcifications type as it is the smallest among the rest of tumour types it should be considered according to well-established characteristics: shape - size - density - number - distribution.

2.2.3. Microcalcifications

Basically, microcalcifications are tiny specks of calcium usually less than 1mm in size and between 0.1 and 0.7 mm in diameter [2]. Microcalcifications sometimes have subtle appearance with hazy borders [3]. However, most studies in the area of mammography agree on describing them showing as bright white spots against the darker background of a mammogram [4] [5].

One of the important characteristics of microcalcifications is that they group into clusters. However, microcalcification clusters are defined differently in several papers. Microcalcification clusters are defined as usually at least 3 microcalcifications within a 1 cm^2 region of a mammogram [3]. A cluster is considered detected if 2 or more microcalcifications are found within the true circle defined by an expert [6]. Gulsrud and Husoy in [7] considered a cluster is to be detected if at least one microcalcification is found within the associated ground truth circle. Furthermore, classifying a mammogram that includes a cluster of microcalcifications is more challenging than doing the same with masses because of their unpredictable shapes, size, density and texture. Subsequently, microcalcifications are divided into two types: benign and malignant [8] as described in the following two sub-sections.

2.2.3.1. Benign Microcalcifications

A benign microcalcification cluster has a smaller number of components than a malignant type, with smaller and rounder shapes. Benign microcalcifications are uniform in size and shape and usually appear as coarse, round or oval shapes. Benign calcifications are homogeneous and have high-density [9]. Their distribution patterns

tend to be scattered or diffuse [10]. Figure 2.3 shows examples of benign microcalcifications of different shapes and sizes.
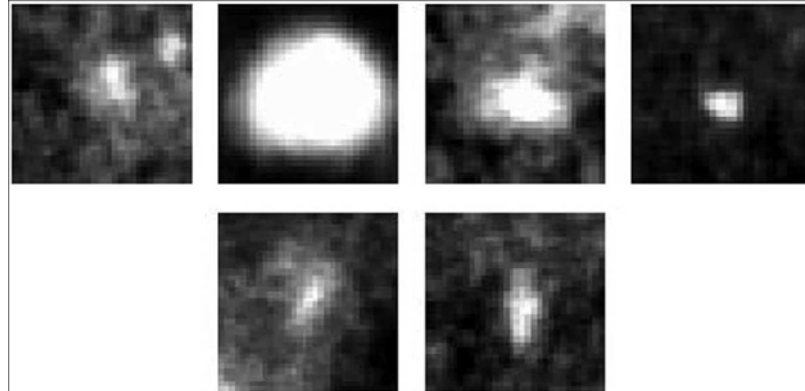
Figure 2.3 Images of 1mm x 1mm vignettes containing individual MCs from benign clusters [11]

2.2.3.2. Malignant Microcalcifications

Malignant microcalcifications within a cluster have a wider variation of sizes compared to the benign type. Also malignant microcalcifications display irregular shapes with a low-density and inhomogeneous appearance [9]. Furthermore, individual malignant microcalcification vary in size and shape, they might appear as microscopic and fine, linear branching or stellate-shapes. Moreover, their distribution pattern is grouped or clustered, and they are innumerable [10].

Malignant microcalcifications are rarely circular in shape and they exhibit sharp increases and decreases in intensity [5]. Figure 2.4 shows examples of malignant microcalcifications of different shapes and sizes.
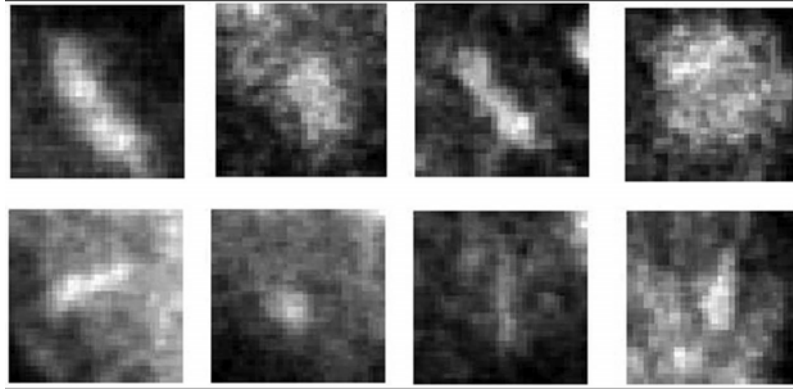
Figure 2.4 Images of 1 mm x 1 mm vignettes containing individual MCs from malignant clusters [11]

2.2.4. Masses

Masses are larger than microcalcifications and are divided similarly into two main types: benign and malignant. Each has characteristics that may help to identify it when detection is attempted. The size of mass lesions considered varies with the study. Cheng and Cui in [4] defined mass lesion sizes vary from 1mm to several centimetres Rafayah *et al.* in [10] divided masses into three sizes: Small (3–15 mm), Medium (15–30 mm), Large (30–50 mm), but the latter case is rare.

Compared with microcalcifications, mass lesions are not only larger but can be of different types and shapes which varies from circumscribed to speculate. Circumscribed mass lesions have relatively well-defined, smooth boundaries, while speculated mass lesions have speculated margins [4]. The benign masses are usually rounded and low-density with smooth, sharply defined margins. On the other hand, malignant masses usually are high-density, stellate, speculated with poorly defined margins [10].

2.3. Segmentation of Microcalcification Regions

Arodez *et al.* [5] proposed a filter design is applied in small field mammography that is sensitive to the typical appearance of individual microcalcifications and detects regions of interest. Small field digital mammograms often contain salt and pepper noise and this method takes this into account. The system works by detecting microcalcifications in two phases and then enhances the contrast of the results. The detection of individual microcalcification in the first phase is done by designing a filter with a value that has a response to the difference of average intensity within the microcalcification and the average intensity outside its borders. The second phase which groups the microcalcifications into clusters, also comprises two parts; first noise removal over the whole mammogram which compares the intensity between pixels by applying median filter and a threshold keeping the isolated pixels only, that represent noise, and then a morphological area opening is applied to remove these isolated pixels. In the second part a discrete wavelet transform is applied to enhance the mammogram image contrast so that microcalcifications are much clearer. This is done by calculating Daubechies wavelets of order 4 and level 5 for the image and using only the 5 sets of the details coefficients with zero for the approximation coefficient before applying the inverse wavelet transform. After detection, a comparison was made with results obtained using the Amira [12] visualisation package to confirm that both results provided similar detected regions of interest for a group of microcalcifications or to connect isolated microcalcification to the rest of the group. This is an interactive evaluation tool which provides a variety of tools to assist in processing 2D and 3D images and specifically microcalcifications are detected using the isolines visualisation technique. This tool is used on the ROI from

the previous step. The isolines technique is used for evaluating microcalcification clusters since it connects pixels with the same brightness as illustrated in Figure 2.1.
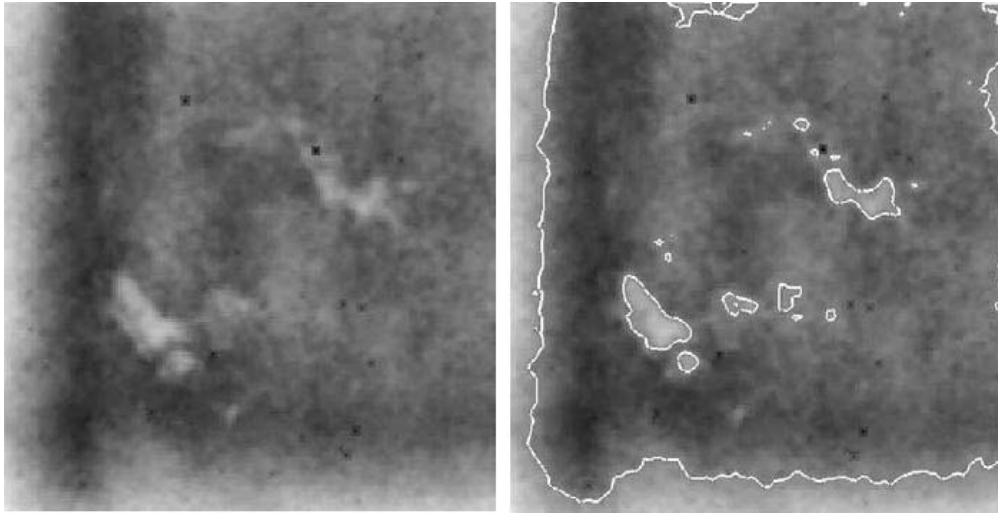
Figure 2.1 Isolines implementation for pixels with similar brightness

The classification method is based on two classification techniques: first the mammogram is classified according to Wolfe breast parenchymal patterns [13]; this classification technique has four categories based on the breast density as an indicator of future cancer risk, they are: primarily fatty 2% (lowest risk), prominent ducts <=25% (low risk), prominent ducts >25% (high risk) and dense fibro-glandular tissue 45% (highest risk). The second classification is based on LeGal classification types for microcalcifications clusters [14], which defines five categories based on the degree of the malignancy.

Melloul and Joskowicz [15] introduced a segmentation method using entropy thresholding. Basically, the method consists of two steps, the first is removing the background tissue, using a multiscale morphological opening operation (morphological top-hat filter). Filtering is performed using a kernel and also changing its size to perform multi-scaling. The kernel is given a size varying from

smallest to largest for each microcalcification. The second is applying the entropy thresholding based on a third-order spatial grey-level dependence matrix to detect individual microcalcifications. This is done using third-order space mean. The threshold that has been used is the one that separates between the background and microcalcifications that have the maximum sum of entropies. This was applied on the Mini-MIAS database achieving a mean detection rate of 93.75% for true positives and 6.25% for false positives with 2% false negatives. The results were evaluated and confirmed by radiologists..

Diyana *et al.* [16] investigated three methods for detecting microcalcifications in mammogram images from the mini-MIAS database and made comparisons of performances and processing times. The algorithms used in this study included a morphological approach, a fractal approach and a high order statistical approach. Prior to applying these methods, a pre-processing stage was performed to extract the breast region from the background using block region growing. The detection algorithms were then applied. The morphological approach implemented opening and P-tile thresholding methods; that is erosion and dilation processes are applied on the same image in order to separate the microcalcifications from the breast tissue. The second fractal method applied divides the image into regions of size 8×8 believed to be suitable for the detection of microcalcification size features and then implements the fractal model on each region. The third high-order-statistical approach applied is based on the characteristic that microcalcifications are bright spots compared with neighbouring pixels. Thus, local intensity maxima are detected and ranked according to a high order statistical test performed over sub-bands obtained from an adaptive wavelet transform. After comparing the results from the

three methods it was found that the morphological approach produced the best results with 74% true positives in 3.20 minutes.

Sentelle *et al.* [17] investigated a rapid, multi-resolution-based approach combined with wavelet analysis to provide an accurate segmentation of possible microcalcifications. This approach was implemented on 25 images obtained from the Digital Database for Screening Mammography (DDSM). An initial multi-resolution approach to fuzzy c-means (FCM) segmentation was employed to quickly distinguish medically significant tissues. Tissue areas chosen for high-resolution analysis were later divided into multiple windows. Each window, wavelet analysis was employed to generate a contrast image, and a local FCM segmentation generated an estimation of the local intensity. A simple two-rule fuzzy system is applied combining intensity and contrast information to derive fuzzy memberships of pixels in the high-contrast, bright pixel class. A double threshold was finally applied to the fuzzy membership to detect and segment microcalcifications.

Stojic *et al.* [18] applied a method for detecting small-sized brighter regions in mammogram images from the mini-MIAS database, based on an adaptive multi-fractal approach for segmentation and visualization of microcalcifications. Cropping images manually into suspicious regions of sizes 128×128 or 256×256 pixels was the first step in the application of their method. This study considered two cases, one of them marked as an easy case for radiologists and the other as a hard case. For the former case it was reported that the tissue is radiology sparse and microcalcifications are visible even to a less-skilled radiologist; by contrast in the latter case the breast tissue is very dense causing very poor contrast between abnormality and surrounding tissue making microcalcifications extremely difficult to detect even by a skilled radiologist. In their study they ascribed several characteristics to microcalcifications.

Basically microcalcifications are small brighter local tissue anomalies in mammograms not belonging to background tissue. From the geometrical interpretation, they are seen as singular sets of points. From the multifractal standpoint they are characterizes by both high and low values as they represent sharp local changes and rare events.

Hadhoud *et al.* in [19] used wavelet decomposition as an enhancement method to remove noise from the mammogram images. An orthogonal wavelet was used to remove redundancy in the information that is represented by the wavelet coefficients; at the same time it provides a corrected reconstruction of the original image. It starts by applying a (unspecified) Daubechies family wavelet decomposition. Then a soft-threshold is applied that involves setting detail coefficients whose absolute values are lower than the threshold to zero and then scaling nonzero coefficients to zero. This eliminates the discontinuity that is inherent in a hard-threshold. The threshold is computed using local statistics from the original mammogram including mean intensity, standard deviation, median value, and minimum value. After thresholding, reconstruction is performed using the original approximation coefficients and the modified detail coefficients.

2.4. Extraction of Features for the Classification of Breast Tissue

Wavelet decomposition was applied in a previous study by Ferreira and Borges in [20] using the mini-MIAS database. Using 'Haar' and 'DB4' wavelets, it was found that extracting the 100 wavelet coefficients largest in magnitude from the approximation included enough wavelet features to represent brighter abnormal objects. Classification of tumour nature (i.e. normal, benign, and malignant) was based on the Euclidean distance. Performances of 83.3% for malignant and 94.4%

for normal tissue were achieved using Haar wavelets with corresponding values of 88.8% and 72.2% using DB4 wavelets.

Sheshadri and Kandaswamy investigated in [21] the extraction of statistical features for the classification of the breast tissue in mini-MIAS mammograms. The classification accuracy for breast tissue of this algorithm is nearly 80% and the results have been inspected and validated by an expert radiologist. The results show the appearance of abnormalities in high density breast tissue. Therefore, the extraction of statistical features for the classification of breast tissue should be investigated further. The algorithm classifies the pixels from the input image into either interior or boundary pixels; the interior pixels include the interior parts of texture regions. Then segmentation is performed by applying region growing to the interior pixels. Basically the classification is based on the values of the texture parameters which are: Average intensity, Average contrast, Smoothness, Third moment, Uniformity and Entropy; and also on the standard parameters defined for image histograms by ACR-BIRADS (American College of Radiology-Breast imaging and Reporting Data Systems). The six statistical features that are used are mean, standard deviation, smoothness, third moment, uniformity, and entropy. Gulsrud and Husoy investigated in [7], a method applied to mammograms from the mini-MIAS database which is based on the extraction of texture features. Their detection rate was 1.5% false positives and about 95% true positives. The extracted features are used to differentiate between textures that include microcalcification clusters and normal tissue. The method employs a single filter whose design is optimized with respect to the Fisher criterion [22]. The Fisher criterion uses mean and variance to achieve good feature separation and provides a smoothing parameter

to be tuned. The tuning of this parameter to optimize the filter requires two sub-images, one with normal tissue and one with clusters of microcalcifications.

2.5. Classification

The method of Sheshadri and Kandaswamy in [3] reaches a true positive detection rate of 100% with a rate of only 1.5% false positive clusters per image from the mini-MIAS database. For the classification of detected clusters as benign or malignant, their CAD system achieved an overall performance rate of about 75%. Basically, this was achieved by manually cropping regions of interest (ROI) from the mammograms and processing these parts only rather than the whole mammogram. After cropping ROIs, feature extraction is applied for segmentation purposes to divide the region into normal tissue or clusters of microcalcifications. Texture feature extraction methods are then applied to differentiate between benign and malignant clusters of microcalcifications. These methods use digital filters with a filter response energy measure that is based on spatial grey level co-occurrence matrices (i.e. second order statistical measures of image variation).

Yu *et al.* in [23] applied a wavelet filter and a Markov random field (MRF) in order to detect microcalcification clusters in mammogram images. The MRF has been utilized in various image processing application related to texture modelling and discrimination. The MRF is a well-known class of parametric image model whose importance deals with a large number of spatial interaction phenomena which can be statistically described by MRFs. In this study 20 mammogram images from the mini-MIAS database were used. First the detection of suspicious regions is based on grey levels in the MIAS database in the range of 175 – 226 grey levels and sizes of microcalcification clusters varying from 6 to as many as 87 pixels. In order to extract

these features from the breast background, a wavelet filter is applied since microcalcification clusters have high contrast with respect to their neighbours as well as containing high frequency components. Then a threshold of the mean pixel value is applied that is set to 10 in order to detect the suspicious regions. In the next stage feature extraction is applied using the least-squares-error Markov random field method proposed by Derin *et al.* [24] in order to identify the texture of the microcalcifications. Edge density is found to be a good feature for discriminating microcalcification clusters from normal regions. For the classification stage, two classifiers were implemented: Bayes and Back Propagation Neural Network (BPNN). The Bayes classifier is a statistical classifier, which is designed to minimize the error when discriminating between classes. On the other hand, the BPNN can achieve lower False Positives rates than Bayes classifiers. As a result, the algorithm performance reached a sensitivity of 92% with an average of 0.75 false positives per image.

Papadopoulos *et al.* in [25] proposed a system that consists of three stages: (1) Detection of microcalcifications clusters; (2) Feature extraction from the clusters; (3) Classification. It is based on a hybrid intelligent system combining rule-based, artificial neural networks (ANNs) and support vector machines (SVMs) with Gaussian kernel function methods. This study applied the proposed algorithm on two datasets for comparison. Using the Nijmegen database, the correct characterization of 44 (52%) malignant clusters and the false characterization of 2 (5.8%) benign clusters was achieved. Using the MIAS database, the correct characterization of 11 (61%) malignant clusters and the false classification of 1 (7.6%) benign clusters was achieved. To summarise, the final results were: a classification rate of 81% for the Nijmegen dataset and 83% for the MIAS dataset.

Songyang and Ling in [26] proposed an algorithm to detect the microcalcification in mammogram images based on wavelet features and neural networks. They utilized median contrast and normalised grey level features obtained by applying the fourth-level Daubechies-orthogonal wavelet transformation to train a feed-forward NN classifier to trace the likelihood map that shows the possibility of the input values being a microcalcification. The resulting algorithm was successful in detecting 94% of the mean true positives at a cost of one false positive per image and 90% of the mean true positives at a cost of 0.5 false positive per image.

Rafayah *et al.* in [10] proposed a computer-aided-diagnosis algorithm using a wavelet analysis and fuzzy–neural approach for detecting the microcalcification in mammogram images. Horizontal, diagonal and vertical detail coefficients from a wavelet decomposition of the image coefficients were extracted for feature vectors. Normalization of the coefficients, energy and feature reductions were carried out. Two classifiers were generated: one processing globally using Neuro-fuzzy classifier using 100 coefficients and the other processing locally on cropped ROIs using 35 coefficients. The classification between normal and abnormal category using 100 coefficients achieved a classification average of 81.4% while classification between benign and malignant calcifications achieved a classification average of 87.5% using the 35 coefficients.

Cheng *et al.* [27] suggested the use of Fuzzy logic and scale space approaches. The first stage of the procedure was to apply a fuzzy-based image enhancement. The regions of interest in each image were manually located as rectangular sub-images that contain a maximum number of microcalcifications. The Laplacian of Gaussian (LoG) filter is then applied on the enhanced images to detect microcalcification clusters. The final result of this study was very effective in locating

microcalcifications achieving a true positive rate of 90% with a false positive rate of 1%. This study was applied on images that are obtained from the Nijmegen database of mammography.

2.6. Summary

The reported previous studies mentioned above have achieved valuable results using several techniques and methods. Moreover, a number of these studies have combined more than one machine learning technique such as neural networks and support vector machines in order to classify between several classes of tumour or to distinguish between microcalcifications and other suspicious objects. This is likely to need a huge computational effort and time consuming training and testing of data. Furthermore, the majority of these studies have utilised the mini-MIAS database to investigate their methods, rather than the MIAS database of original size images which has the advantage of higher resolution with the microcalcifications clearer to study besides other mammographic databases such as Nijmegen and DDSM. In a number of the studies that have been mentioned above the wavelet transform has been used in various ways such as for image enhancement, image segmentation and feature extraction in a few. Most of these studies have included the detailed coefficients, which include the horizontal, diagonal and vertical coefficients, but a few studies have utilised only the approximation coefficients that represent reduced resolution images. Moreover, a limited number of wavelet types have been investigated, mainly the Haar wavelet and the Daubechies wavelet from order 2 and 4. Since few studies have used the wavelet transform for feature extractions most other studies mainly focus on using statistical features combined with a machine learning technique as mentioned in the previous reported studies. These studies

achieved not more than 95% of microcalcification detection and 94% of classification.

However, the work that has been presented in this study did manage to tackle most of these problems in order to achieve a high accuracy of classification using direct methods and techniques. In Chapter 3, a segmentation technique that has been adapted from [28] has been modified from detecting masses to detecting microcalcifications using only the mean pixel values to compare between a central area and its surroundings. This is done on cropped regions of interest (ROI) from different sizes that represent clusters of microcalcifications and individual microcalcification using the original MIAS database of mammography. Then in Chapter 4, the wavelet transform has been utilised at this stage for feature extraction using only the approximation coefficients. This scheme was adapted from [20] and modified to extract features from black and white images that are thresholded instead of grey scale images. Thus, the feature extraction method was applied on cropped ROI from the original MIAS instead of the mini-MIAS. In addition, there are six different wavelet types that have been investigated from levels 1 and 2 of decomposition. Chapter 5 explains the process of a classification method based on the wavelet transform features using support vector machine (SVM) that has been adapted from different areas of study [29, 30] and modified to suit this area of research. This process investigates the classification between normal breast tissue and abnormal areas that may contain microcalcifications.

References:

1. *Mammographic Image Analysis Society.* [cited 2005 october]; Available from: http://www.wiau.man.ac.uk/services/MIAS/MIASweb.html.

2. Bocchi, L. and Nori, J., *Shape analysis of microcalcifications using Radon transform.* Medical Engineering & Physics, 2007. **29**(6): pp. 691-698.

3. Sheshadri, H.S. and Kandaswamy, A., *Computer Aided Diagnosis of Digital Mammograms.* Information Technology Journal, 2006. **5**(2): pp. 342-346.

4. Cheng, H.D. and Cui, M., *Mass lesion detection with a fuzzy neural network.* Pattern Recognition, 2004. **37**(6): pp. 1189-1200.

5. Arodz, T., Kurdziel, M., Popiela, T.J., Sevre, E.O.D., and Yuen, D.A., *Detection of clustered microcalcifications in small field digital mammography.* Computer Methods and Programs in Biomedicine, 2006. **81**(1): pp. 56-65.

6. Strickland, R.N. and Hahn, T., *Wavelet transform for detecting microcalcifications in mammograms.* IEEE Transactions on Medical Imaging, 1996. **15**(2): pp. 218-229.

7. Gulsrud, T.O. and Husoy, J.H., *Optimal filter-based detection of microcalcifications.* Biomedical Engineering, IEEE Transactions on, 2001. **48**(11): pp. 1272-1281.

8. Liyang, W., Yongyi, Y., Nishikawa, R.M., and Yulei, J., *A study on several Machine-learning methods for classification of Malignant and benign clustered microcalcifications.* Medical Imaging, IEEE Transactions on, 2005. **24**(3): pp. 371-380.

9. Frigas, A.N. *Microcalcifications resource site.* 2009 [cited 2009 october]; Available from: http://www.infoacademy.gr/microcalc/.

10. Rafayah, M., Qutaishat, M., and Abdallah, M., *Breast cancer diagnosis system based on wavelet analysis and fuzzy-neural.* Expert Systems with Applications, 2005. **28**(4): pp. 713-723.

11. Rogova, G.L. and Stomper, P.C., *Information fusion approach to microcalcification characterization.* Information Fusion, 2002. **3**(2): pp. 91-102.

12. Mercury computer system Inc. *Advanced 3D Visualisation and Volume Modelling.* [cited 2006 March]; Available from: www.amiravis.com.

13. Wolfe, J., *Breast parenchymal patterns and their changes with age.* Radiology, 1976. **121**(3): pp. 545-552.

14. LeGal, M. and Ghavanne, G., *Valeur diagnostique des microcalcification groupees decouvertes par mammographies.* Bulletin du cancer, 1984. **71**: pp. 57-64.

15. Melloul, M. and Joskowicz, L. *Segmentation of microcalcifications in X-ray mammograms using entropy thresholding.* in Proceeding of the 16th International Congress on Computer-Assisted Radiology and Surgery. 2002.

16. Diyana, W.M., Larcher, J., and Besar, R., *A comparison of clustered microcalcifications automated detection methods in digital mammogram.* Proceedings of IEEE International Conference on Acoustics, Speech, and Signal Processing, 2003. **2**: pp. 385-388.

17. Sentelle, S., Sentelle, C., and Sutton, M.A., *Multiresolution-Based Segmentation of Calcifications for the Early Detection of Breast Cancer.* Real-Time Imaging, 2002. **8**(3): pp. 237-252.

18. Stojic, T., Reljin, I., and Reljin, B., *Adaptation of multifractal analysis to segmentation of microcalcifications in digital mammograms.* Physica A: Statistical Mechanics and its Applications, 2006. **367**: pp. 494-508.

19. Hadhoud, M., Amin, M., and Dabbour, W., *Detection of Breast Cancer Tumor Algorithm using Mathematical Morphology and Wavelet Analysis.* Proceeding of the first ICGST International Conference on Graphics, Vision and Image Processing, 2005. **5**: pp. 75-80.

20. Ferreira, C.B.R. and Borges, D.L., *Analysis of mammogram classification using a wavelet transform decomposition.* Pattern Recognition Letters, 2003. **24**(7): pp. 973-982.

21. Sheshadri, H.S. and Kandaswamy, A., *Experimental investigation on breast tissue classification based on statistical feature extraction of mammograms.* Computerized Medical Imaging and Graphics, 2007. **31**(1): pp. 46-48.

22. Fukunaga, K., *Introduction to statistical pattern recognition (2nd ed.).* 1990, San Diego, CA, USA: Academic Press Professional, Inc. 592.

23. Yu, S.N., Li, K.Y., and Huang, Y.K., *Detection of microcalcifications in digital mammograms using wavelet filter and Markov random field model.* Computerized Medical Imaging and Graphics, 2006. **30**(3): pp. 163-173.

24. Derin, H., Elliot, H., and Kuang, J. *A new approach to parameter estimations for Gibbs random fields*. in Proceedings of IEEE international conference acoustics, speech, and signal processing. 1985. Tampa, FL.

25. Papadopoulos, A., Fotiadis, D.I., and Likas, A., *Characterization of clustered microcalcifications in digitized mammograms using neural networks and support vector machines*. Artificial Intelligence in Medicine, 2005. **34**(2): pp. 141-150.

26. Songyang, Y. and Ling, G., *A CAD system for the automatic detection of clustered microcalcifications in digitized mammogram films*. Medical Imaging, IEEE Transactions on, 2000. **19**(2): pp. 115-126.

27. Cheng, H.D., Wang, J., and Shi, X., *Microcalcification detection using fuzzy logic and scale space approaches*. Pattern Recognition, 2004. **37**(2): pp. 363-375.

28. Kom, G., Tiedeu, A., and Tiedeu, M., *Automated detection of masses in mammograms by local adaptive thresholding*. Computers in Biology and Medicine, 2007. **37**(1): pp. 37-48.

29. Qahwaji, R. and Colak, T., *Automatic Short-Term Solar Flare Predection Using Machine Learning and Sunspot Associations*. Solar Physics, 2007. **241**(1): pp. 195-211.

30. Colak, T. and Qahwaji, R., *Automated Prediction of Solar Flares Using Neural Networks and Sunspots Associations*. Advances in Soft Computing, 2007. **39**: pp. 316-324.

Chapter 3

Microcalcifications Segmentation

3.1. Introduction

Segmentation in computer vision is the term used for partitioning an image into multiple non overlapping regions. Often, these regions are divided into two classes, foreground regions of interest and the remaining background region. In the field of mammography the process of segmentation is used at different stages to separate the breast region from the non-breast region, to remove labels from the image and to separate abnormal breast tissue from normal breast tissue [1-5]. These have been applied in previous studies as discussed in the previous chapter, while in this chapter we focus on applying a direct method of segmentation to a region of interest within an image. This is to eliminate the background breast tissue and keep only suspicious objects or potential microcalcification in the current case. Applying such a method on ROI images that hold normal and abnormal breast tissue would help in the following step of features extraction. This process is performed to locate suspicious objects within an ROI image and specifically microcalcifications. However, these regions still need to be differentiated to assist radiologists in the final diagnosis. This technique basically applies a filter on an image to be scanned to compare a middle area with its surroundings. Thus, there will not be any additional preceding steps for enhancement as image pre-processing.

This chapter is organised as follows. Section 2 outlines the selection of data for the subsequent analysis steps. Section 3 presents a segmentation method involving the

design of detection filters to separate the foreground "microcalcifications" from the background "breast tissue". This section is divided into two subsections describing the implementations of square and circular filters. Section 4 summarises the chapter with examples of the results that have been obtained from the experiments.

3.2.   Regions of Interest (ROI)

Regions of interest are the parts of the mammograms where radiologists find abnormalities in the breast tissue such as microcalcifications and masses. However, finding these regions automatically is not easy given that these abnormalities are small in size and may have similar contrast and brightness to neighbouring regions of the breast tissue, making them difficult to spot with the human eye.

In this research we look at how using cropped regions of interest reduces the time spent on the experiments compared with processing full sized mammograms, as well as focusing the analysis on regions of interest, cropped manually, which contain suspicious objects that need to be studied; rather than getting complex features from all over the mammogram image as well as reducing the number of false positives. The idea of processing a full mammogram image, covering all the possibilities that can be identified, analyzing and storing, then awaiting confirmation by the radiologists can be highly beneficial for such systems. However, such methods consequently replace the radiologist's opinions in selecting and analyzing suspicious regions from the original images. Clinically, digital mammography is only considered as a second opinion and complementary to the decisions of the radiologists.

This experiment has used the full MIAS database. In particular, 20 digital mammogram images that contain microcalcifications and 50 other digital

mammogram images that contain normal, cancer free, breast tissue have been used for this study.

The sizes chosen for the cropped regions are powers of two since this is compatible with the usual wavelet transform processing which reduces the width and height of the image by half at each level. This will be explained later in Section 4.2 on the discrete wavelet transform.

Two sets of cropped regions of interest were produced. The first set was cropped manually and have different sizes to suit the sizes of a single cluster of microcalcifications, as highlighted in the MIAS database, and include: eight images of size of 128×128, nine images of size 256×256, seven images of size 512×512 and one image of size 1024×1024. There are 25 regions of interest containing clusters of microcalcifications and 50 regions of interest containing normal tissue. The normal ROI images have the same sizes as the abnormal ROI images.

The second set of cropped ROI images of size 32×32 include individual microcalcification and were acquired from previous studies in [6] and [7]. This is done by applying two filters, one inside the other, using a size of 9×9 for the inner mask and 13×13 for the outer mask. The average intensity of the inner area of the central area should be greater than other neighbours. As well as the average of the inner filter should be greater than the surrounding area. This is to increase the possibility of detected potential microcalcification. After that, the calculation of the mean and standard deviation for the inner area is applied as well as pixel intensity. These three values are then considered as an input for a feedforward neural network. This neural network is applied to find out the threshold value that separates low level intensity and artefacts from microcalcifications; using three inputs (mean, standard deviation and pixel intensity), one hidden layer (three hidden nodes) and one output

that is the threshold value. An example is shown in Figure 3.1. The total number of these cropped microcalcification regions is 220. An equal number of normal regions were also manually cropped to a size of 32 × 32.

Figure 3.1 Region of interest of size 32×32 containing microcalcifications.

3.3. Image Thresholding

In this research, to be able to study the abnormalities (i.e. microcalcifications) they have to be separated from its surrounding in order to be analysed and examined. Therefore, a segmentation stage is needed which basically partitions the image into multiple segments or non-overlapping sets of pixels [8]. A thresholding based approach is the simplest method of segmentation, which when applied on greyscale images, creates binary images [8]; where in this work one binary value represents potential abnormality and the other binary value represents background. Moreover, further thresholding investigation has been done on 8-bit images keeping the background in black and the detected objects with its original grey-scale colour. This would provide more information out of the suspicious objects in the following chapter. The thresholding process basically provides selected regions for the next stage of feature extraction; to avoid the overhead of extracting and analysing features over the entire image.

The implementation of the thresholding technique has been tested in two forms. First it has been applied to full mammogram images using a square filter. In the second implementation the thresholding method has been modified to be more focused and applied on ROI images with circular filters.

3.3.1. Using Square Filters

This section describes the first test done on a full mammogram image for microcalcifications detection. This thresholding approach has been adapted from a previous study by Kom *et al.* in [9] that investigated breast masses, which are larger scale abnormalities, and modified it to fit with this study and especially the much smaller microcalcifications.

This segmentation method uses a filter with two square windows, one inside the other, as shown in Figure 3.2.
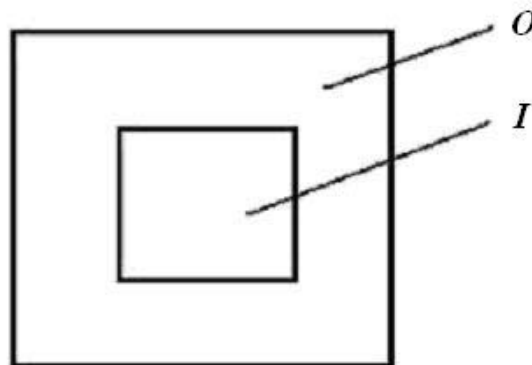
Figure 3.2 Square windows filter used in the adaptive thresholding approach to microcalcification detection.

In Figure 3.2, *I* represents the inner window with a size of 5 × 5 pixels and *O* represents the surrounding border with a size of 20 × 20 pixels. These sizes were chosen empirically after testing several sizes for both the inner and outer window

including 2×2, 3×3, 4×4, 5×5 and 6×6 for the inner window and 10×10, 13×13, 15×15, 18×18, 20×20 and 22×22 for the outer window. These filter sizes are more suitable for application on large mammogram resolutions rather than small resolution mammograms. The chosen sizes gave the best detection covering all the microcalcification peaks for a sample of images within a cluster. These two windows are scanned over the whole mammogram image and at each location the averages of the inner and border regions are calculated. The following criterion is applied to detect abnormal peaks in intensity from background tissue.

$$\text{IF } ((I > m) \text{ and } (I > O + t)) \text{ pixel} = 255 \qquad \text{Else pixel} = 0 \qquad \text{(eq. 3.1)}$$

Here I is the inner window intensity average, m is the minimum intensity value of microcalcifications, taken to be 120 after checking all microcalcifications pixel intensities in mammogram images from the MIAS database, to further confirm this value Adobe Photoshop is subjectively tested on microcalcifications; O is the outer boundary intensity average and t is a second intensity threshold value that was also found empirically and set equal to 10 when it was compared to other threshold values. An evaluation will be presented in section 3.3.2 comparing the square filter shape with circular filter shape using different threshold values.

There are two parts to this criterion used to decide whether to label the centre pixel with the value 255 to indicate a potential microcalcification pixel. The first part is a simple comparison between the inner window of pixel intensity average and the minimum intensity value of microcalcifications m. However, the density of breast tissue varies between each individual case and microcalcification can be found in regions with different background in different parts of a breast and in different

mammograms. Therefore, to take account of this variation the second condition was added. Only if the inner average exceeds the border average by some minimum amount t, found after extensive experiments to be equal 10, is the current location marked as a possible abnormal region.

Figures 3.3 - 3.6 are illustrations from applying the square threshold on full mammogram images showing the original mammogram before and after the segmentation process. Other examples in Figure 3.7 are showing the location of the detected microcalcifications and other suspicious objects from the circular highlight made by the MIAS database experts. It is shown that microcalcifications within the highlighted areas made by the experts are detected. However, some other particles are detected too in other different areas as is clearly visible in Figure 3.7 (b) as well as in the other images, on close inspection. More examples of full mammograms in Figure 3.8 are available with close-ups of some cases in Figure 3.9, showing how the detection technique could also identify other objects that have similar characteristics to microcalcifications that are outside of the circle that contains the microcalcifications. This similarity could include shape, size or pixel intensity that should be tackled and solved.
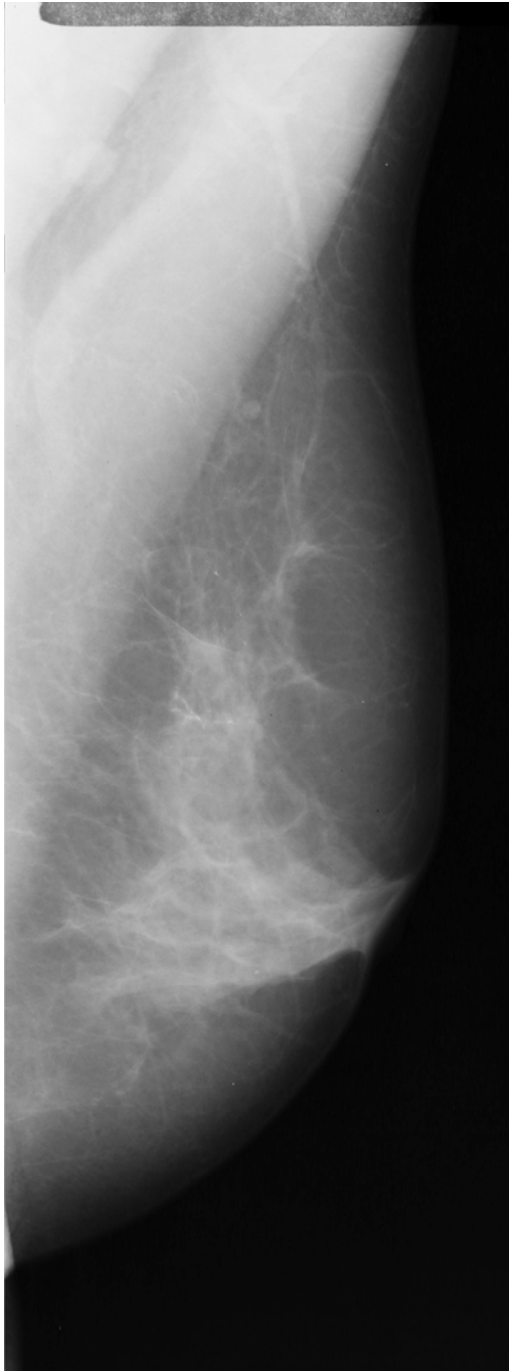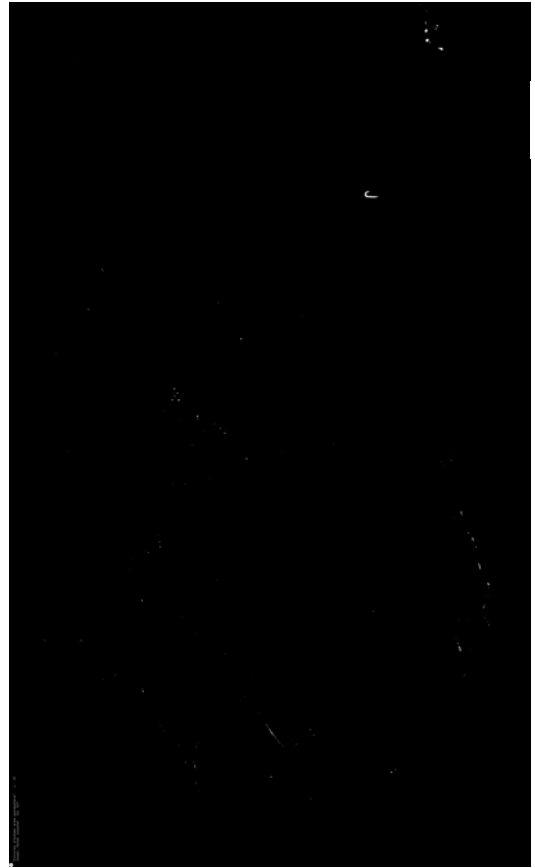
(a) Original Mammogram (mdb213)   (b) Detected microcalcifications within a full mammogram and other artefacts

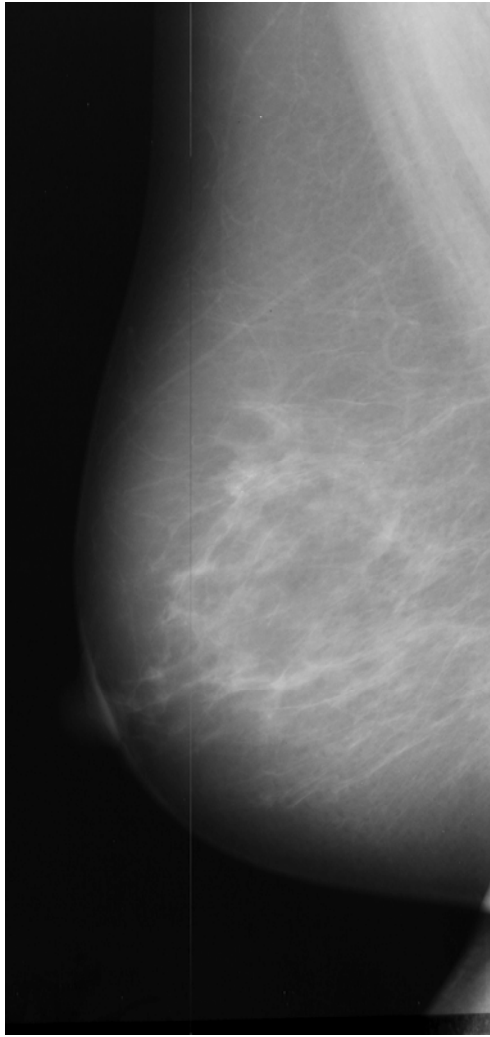**Figure 3.3** Segmentation process exmaple from full mammogram (mdb213)
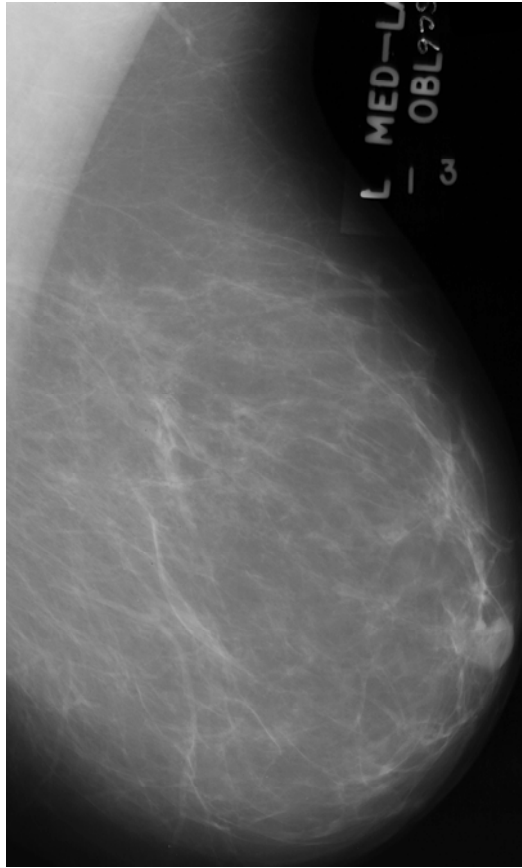
(a) Original Mammogram (mdb231)
(b) Detected microcalcifications within a full mammogram and other artefacts

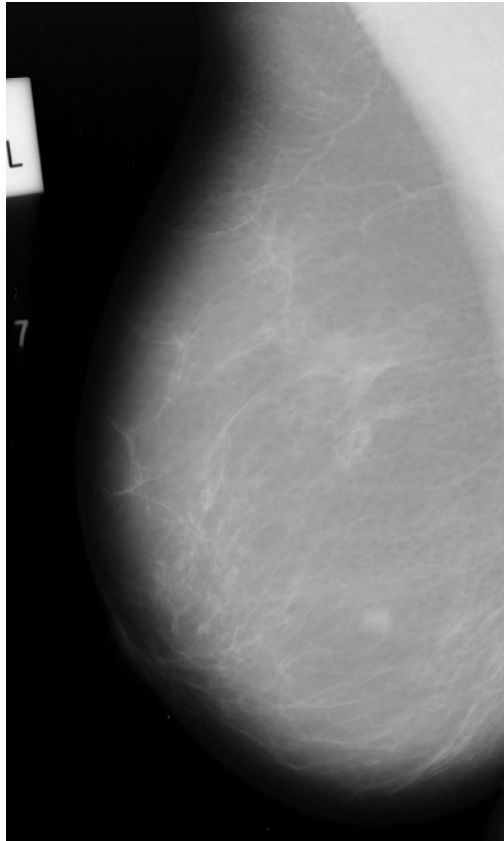**Figure 3.4** Segmentation process exmaple from full mammogram (mdb231)
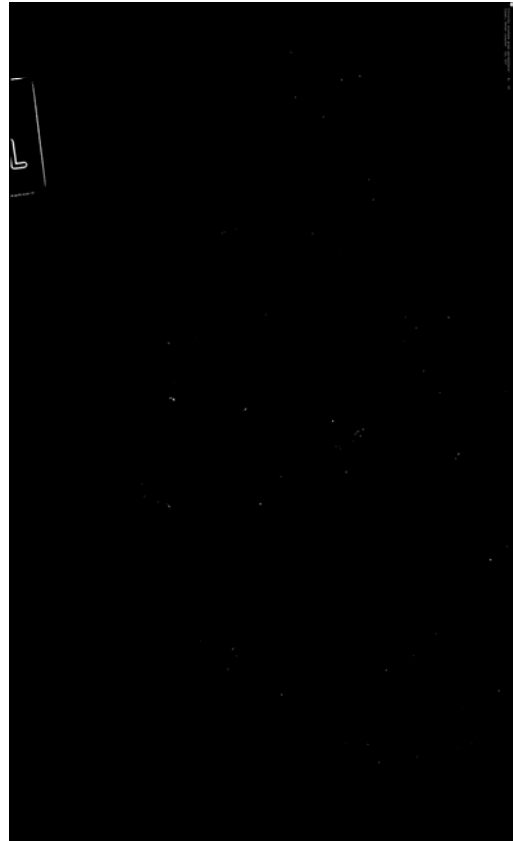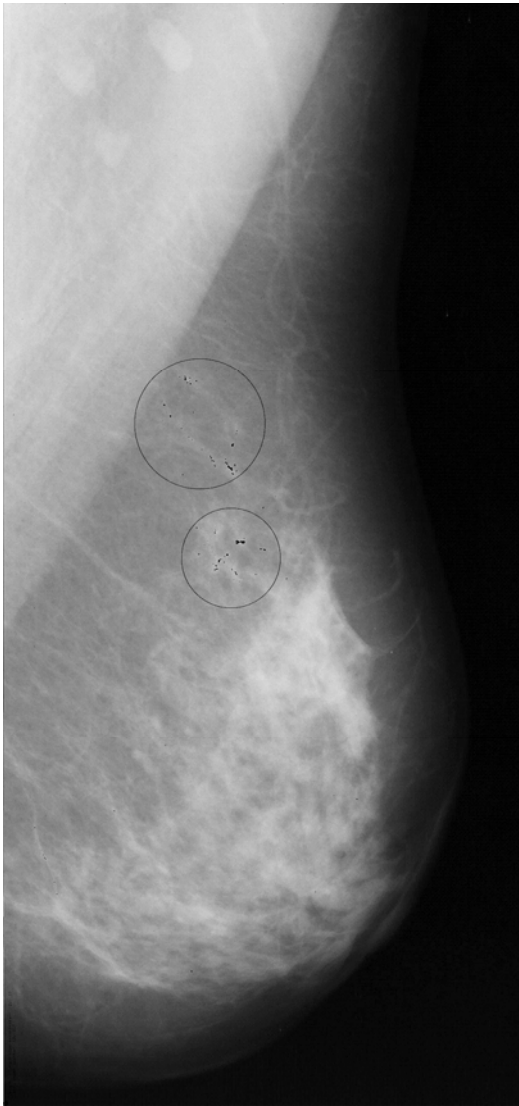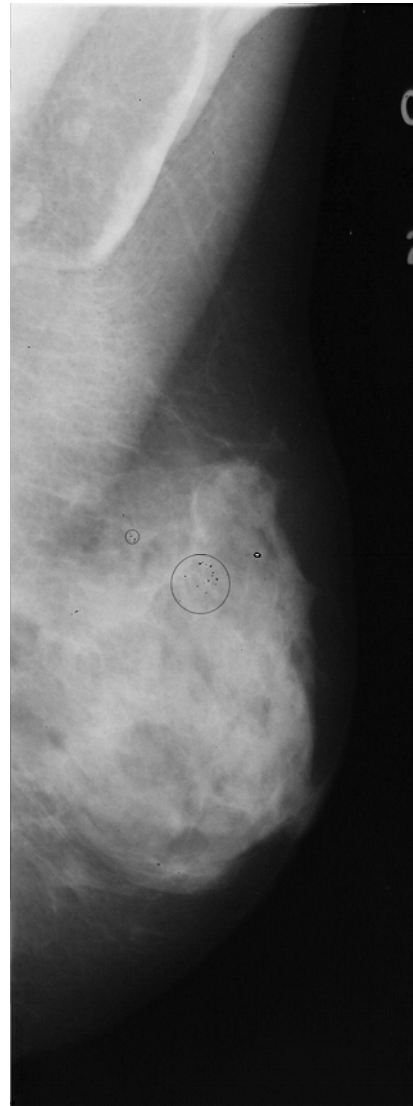
(a) Original Mammogram (mdb238) (b) Detected microcalcifications within a full
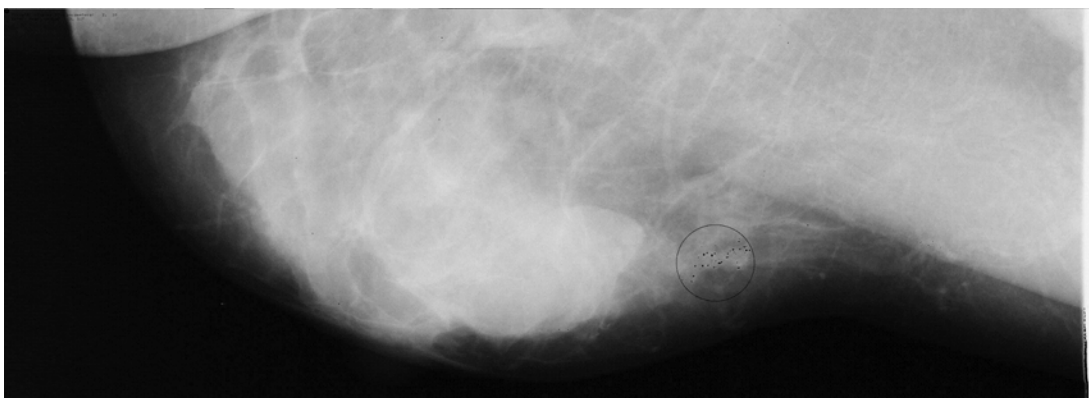mammogram and other artefacts

Figure 3.5 Segmentation process exmaple from full mammogram (mdb238)

(a) Original Mammogram (mdb256)   (b) Detected microcalcifications within a full
                                             mammogram and other artefacts

Figure 3.6 Segmentation process exmaple from full mammogram (mdb256)
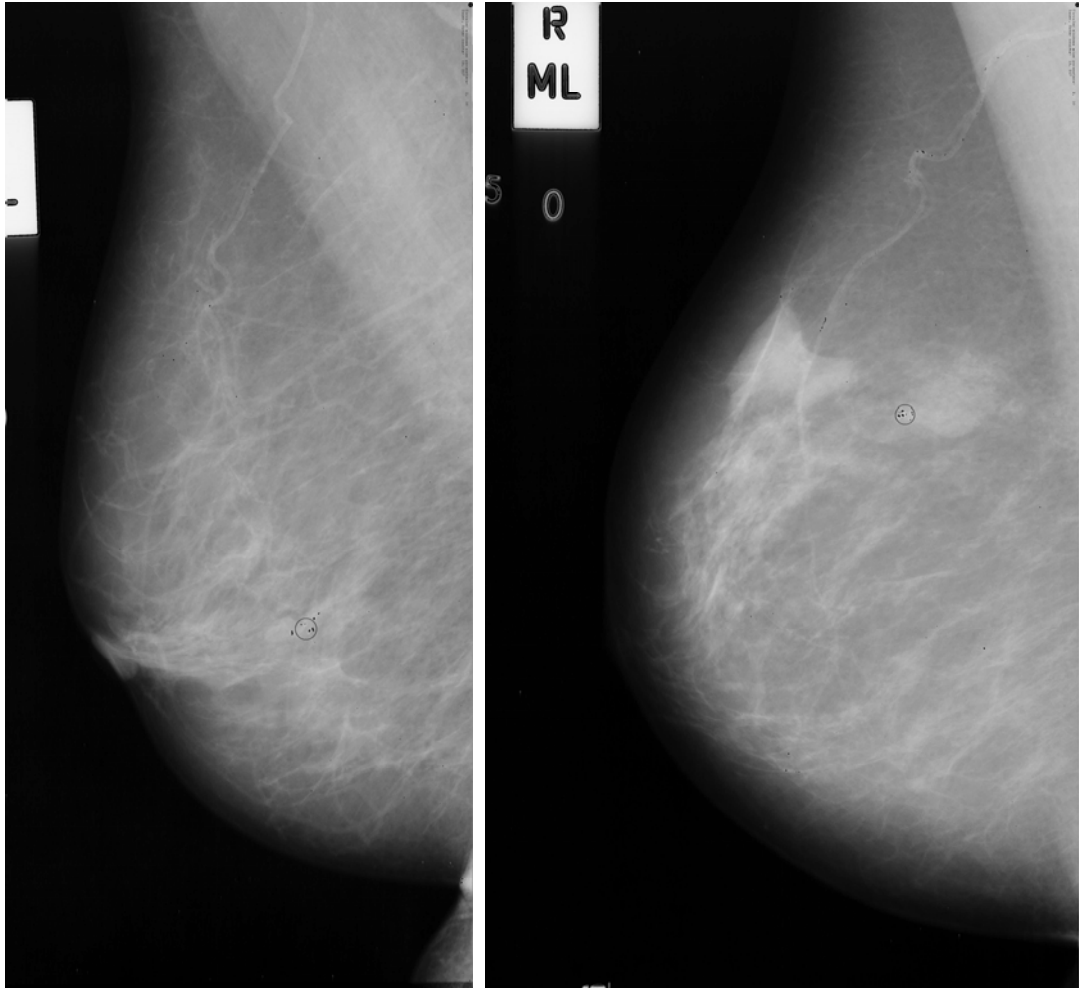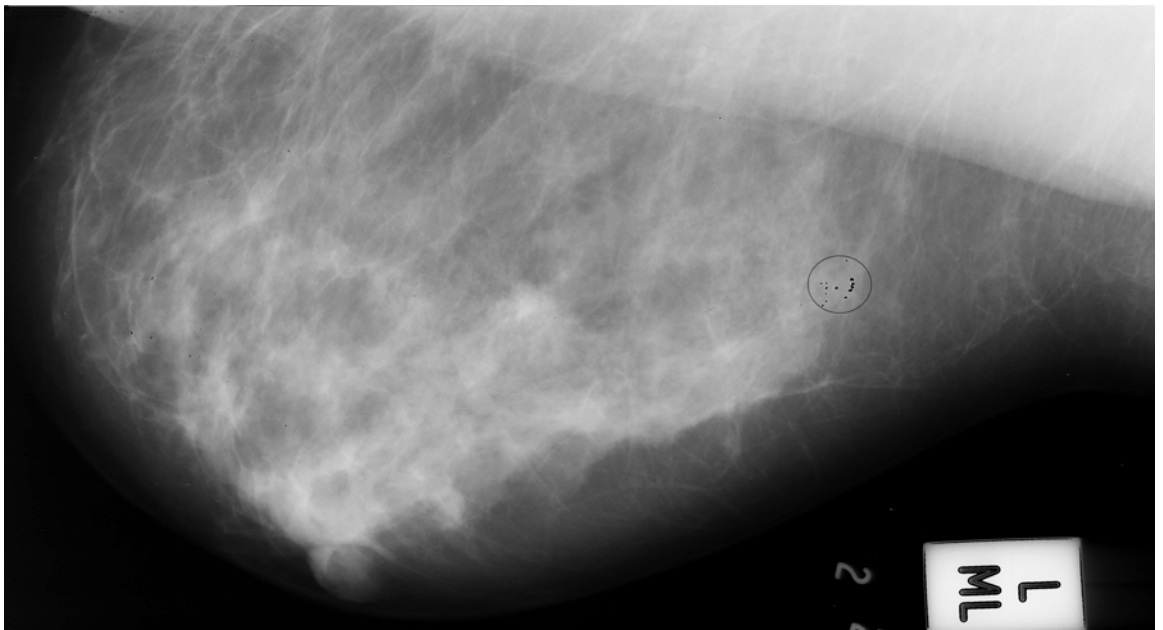
(a) mdb249lm   b) mdb223ls

(c) mdb241ls

Figure 3.7 Results from the first implementation of square threshold, where (a) & (b) contain 2 regions of interest and (c) contains 1 region of interest
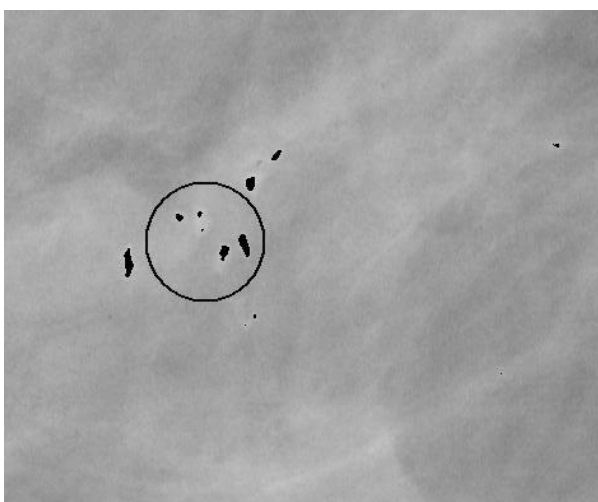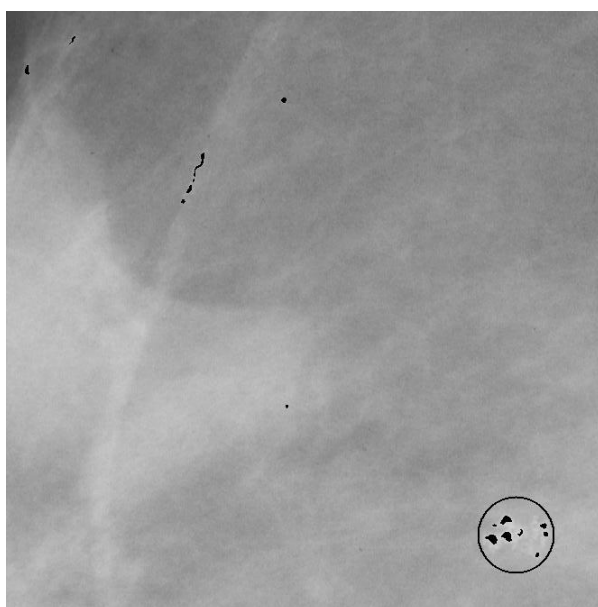
(a) mdb252rm

(b) mdb248rl

(c) mdb219ll

Figure 3.8 Results from the first implementation of the threshold technique

(a) Close up from mdb252rm

(b) Close up from mdb248rl

Figure 3.9 A close up from to two mammograms in (a) and (b) showing the detection of other artefacts detected

3.3.2. Using Circler Filters

In this section a further modification made to the filter is described. This involved changing the shape of the filter's windows from square to circular; since the circular filter has a symmetrical shape with no directional figure, it has a closer match to a microcalcification's shape. This type of filter was applied on regions of interest to let the filters scan only specific areas rather than scanning the whole mammogram. This way the process of the filter will be more focused on vital parts.

The choice of circular filter shape was made principally to reduce any directional sensitivity in the process which could be introduced by using square or rectangular windows. Inevitably, the circular window is an approximation and the smaller the size, the greater the departure from a smooth circular shape. The illustration in Figure3.10 shows the filter windows that have been used on the ROI images in this experiment with radius of 1.5 pixels for the inner filter window and 11 pixels for the outer window.
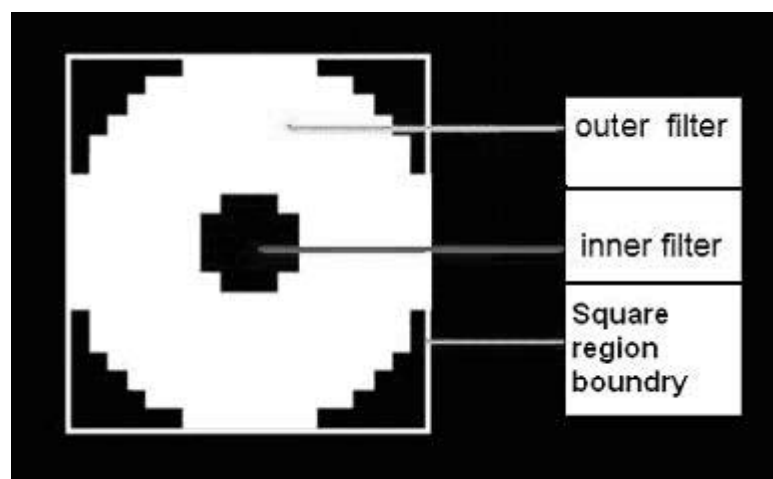

Figure 3.10 Circular window filter

These sizes were chosen empirically to approximate the previous filter size, and these filter radii that have been tested are 1.5, 2, 2.5, 3.5 and 4 for the inner window and 12, 11, 9 and 8 for the outer window. Figure 8 shows implementation results from different window sizes when applied on a single ROI image and illustrates how microcalcifications are detected on some images and missed on others. The size of the side of the square region bounding the circular windows is equal to twice the outer radius plus one for the centre of the circle.

This circular filter, which is closer to the shape of microcalcifications, was applied to two sets of regions of interest. The first contains 75 regions of interest that are focused on clusters of microcalcifications and the second set contains 440 regions of interest that are focused on individual microcalcifications. Figures 3.11 and 3.12, show two example images. The first example is showing the original image before and after the segmentation process using radii size of 1.5×1.5 and 11×11 for the inner and outer filters respectively. This ROI case, mdb223, is from the first dataset, with a size of 128×128. The example in Figure 8 shows, mdb211 ROI case, after applying different sizes of inner and outer filters to compare the amount of microcalcifications that are detected.
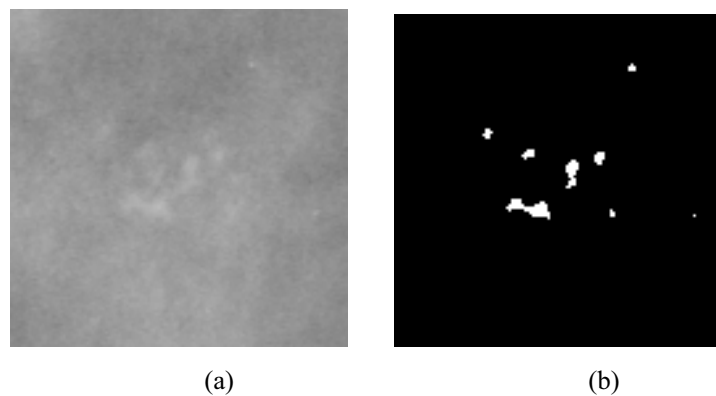

(a)   (b)

Figure 3.11 Region of interest from mdb223 with size of 128×128 ROI (a) original image, (b) after segmentation using inner and outer filters of (1.5, 11)
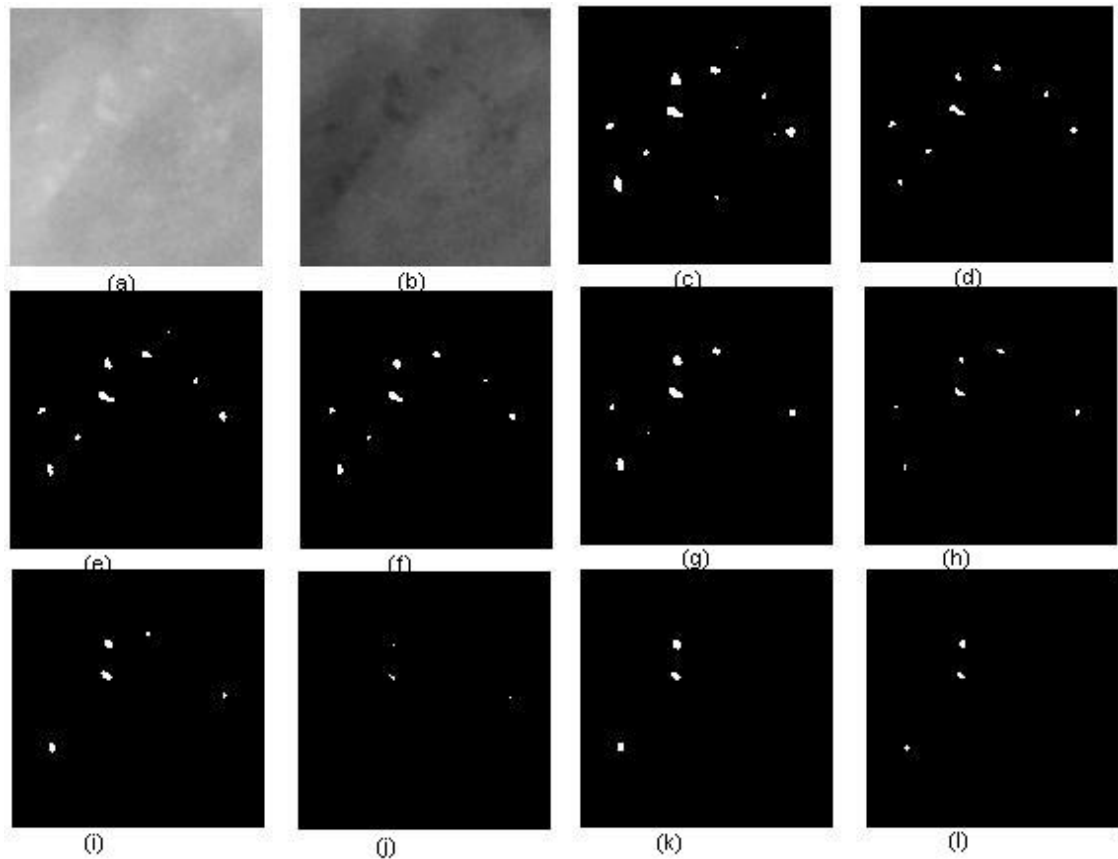
Figure 3.12 Region of interest from mdb211. (a) Original image. (b) Inverted intensity image. Applying different filter inner and outer radius sizes (c) 1.5, 11 pixels, (d) 1.5, 9 pixels, (e) 1.5, 8 pixels, (f) 2, 9 pixels, (g) 2.5, 11 pixels, (h) 2.5, 8 pixels, (i) 3.5, 11 pixels, (j) 3.5, 8 pixels, (k) 4, 12 pixels, (l) 4, 10 pixels

The best result in this set for thresholding the breast tissue "background" from the foreground (i.e. microcalcifications) is shown in Figure 3.8 (c). The original image is also shown inverted in Figure 3.8 (b) as this may show microcalcifications clearer to the human eye. More examples for different ROI sizes are illustrated below in Figures 3.13, 3.14 and 3.15 using the filter radius of 1.5 pixels for the inner window and 11 pixels for the outer window.
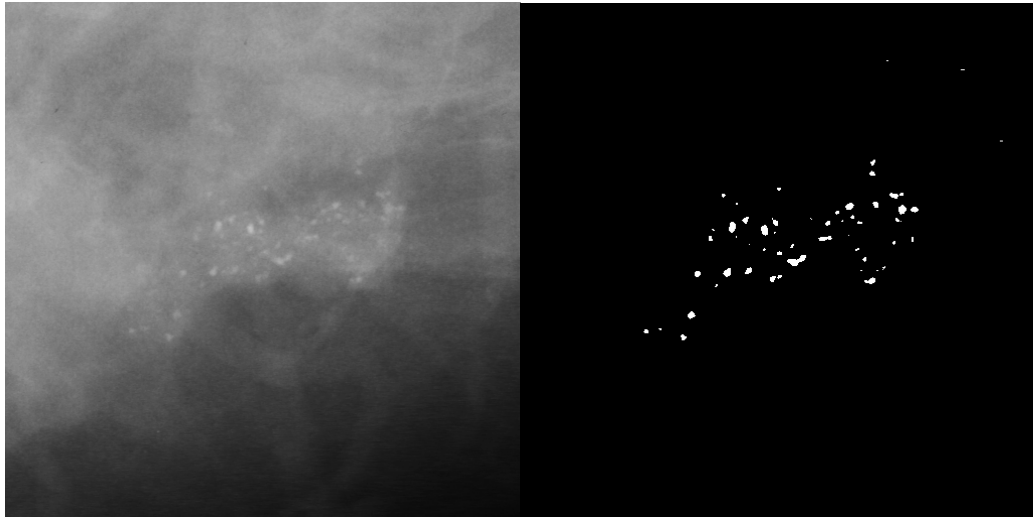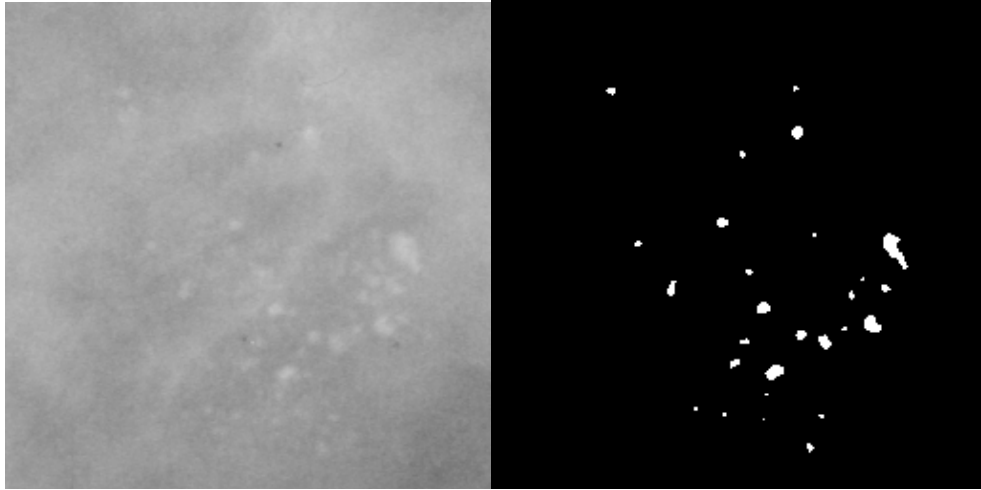
(a) Segmented ROI image of size 512 × 512, before and after
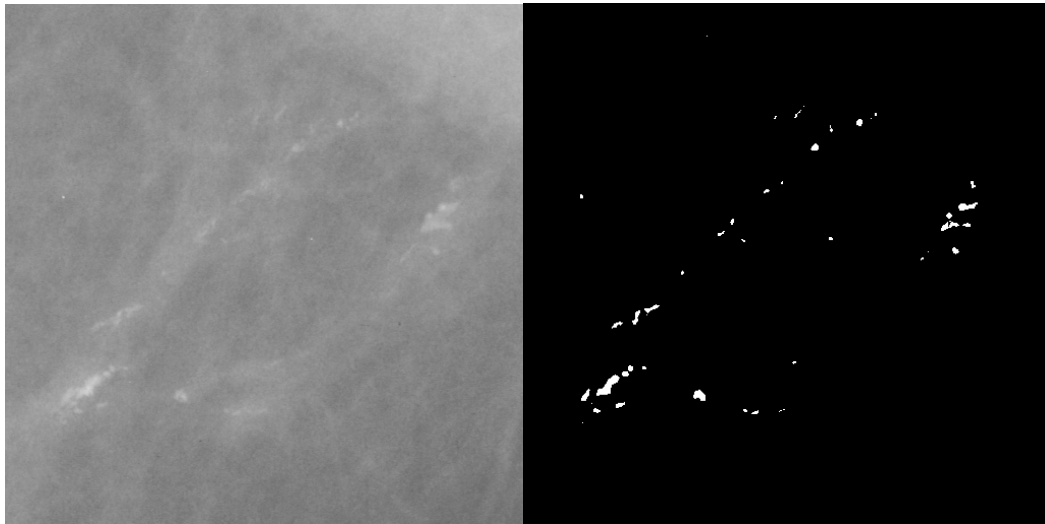
(b) Segmented ROI image of size 512 × 512, before and after

Figure 3.13 Two examples from the ROI size of 512 × 512 (a) mdb241, (b) mdb249

(a) Segmented ROI image of size 256 × 256, before and after
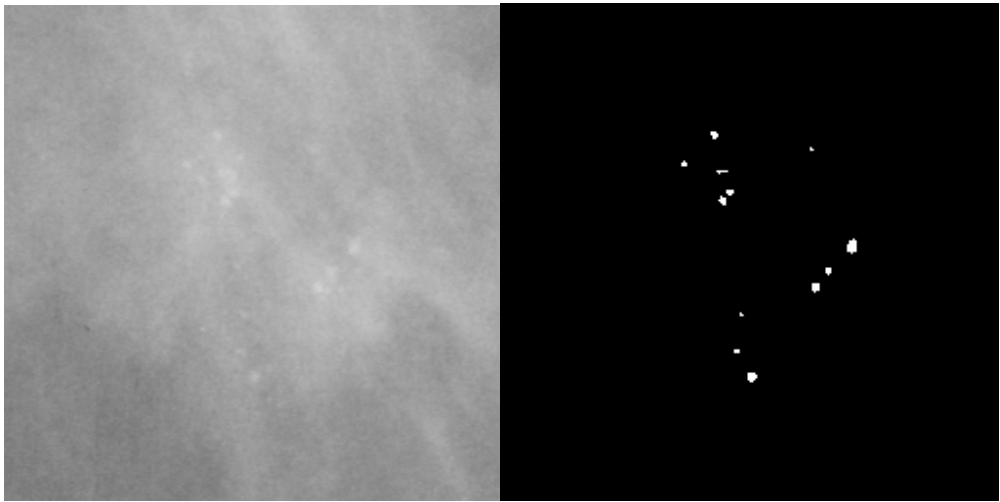
(b) Segmented ROI image of size 256 × 256, before and after

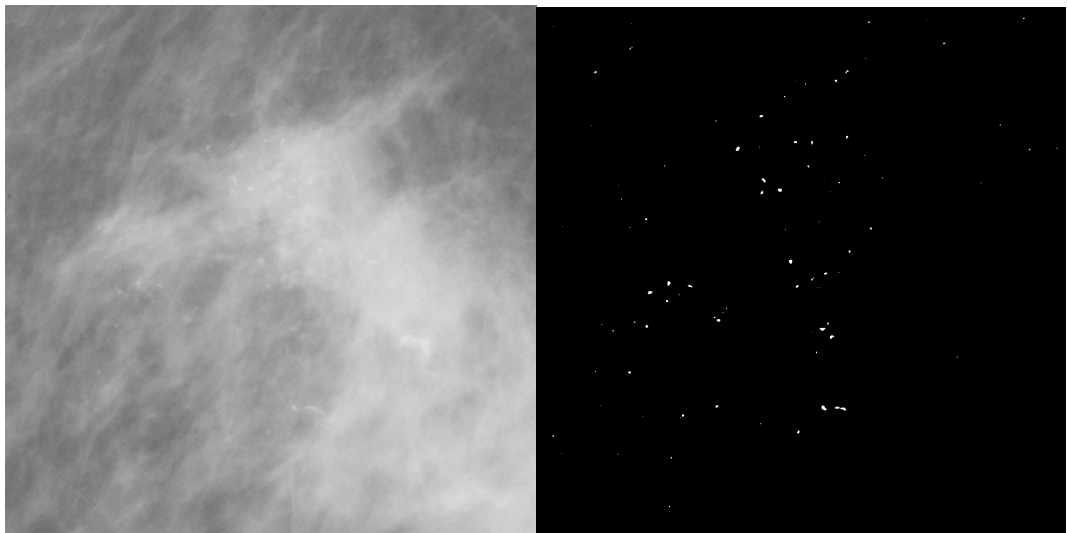**Figure 3.14** Two examples from the ROI size of 256 × 256 (a) mdb223, (b) mdb238

Figure 3.15 Illustration of largest ROI of 1024 × 1024 before and after thresholding

The second dataset that includes 32×32 pixel size ROI images, generated and cropped by AbuBaker *et al.* in [7], are also segmented using the same filter sizes for the inner and outer window. Examples for this ROI size are shown in Figure 3.12. Moreover, an example is provided in Figure 3.17 showing a case of the application of thresholding filters on connected microcalcifications, making them very close to one another or overlapping within the same area. Such cases were cropped individually as mentioned in section 3.2 making each microcalcification centred in the image. This case is also thresholded using the same filters radii of 1.5 pixels for the inner window and 11 pixels for the outer window.
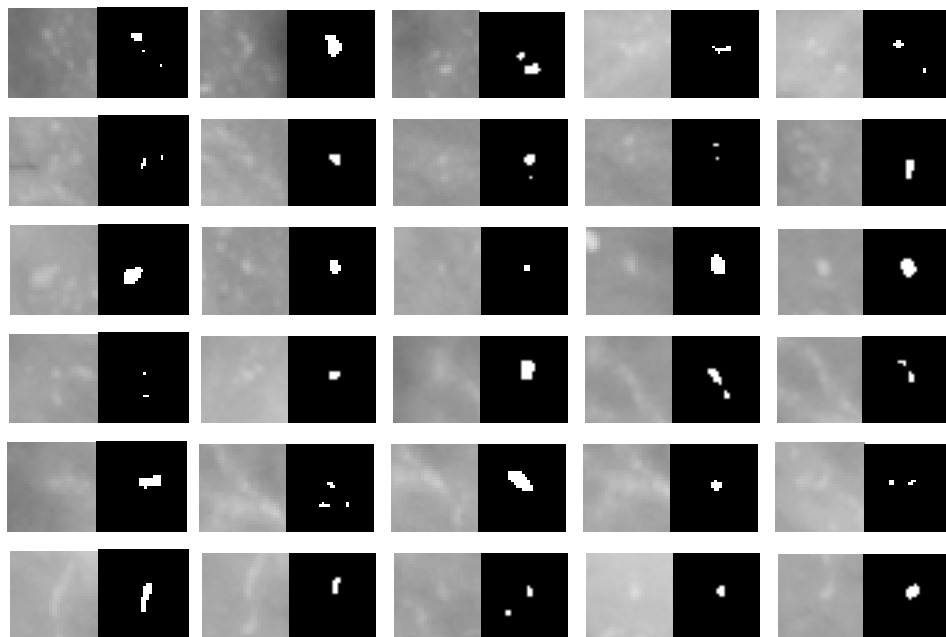

Figure 3.16 Several examples of thresholding, before and after, on 32×32 ROI images of individual microcalcification
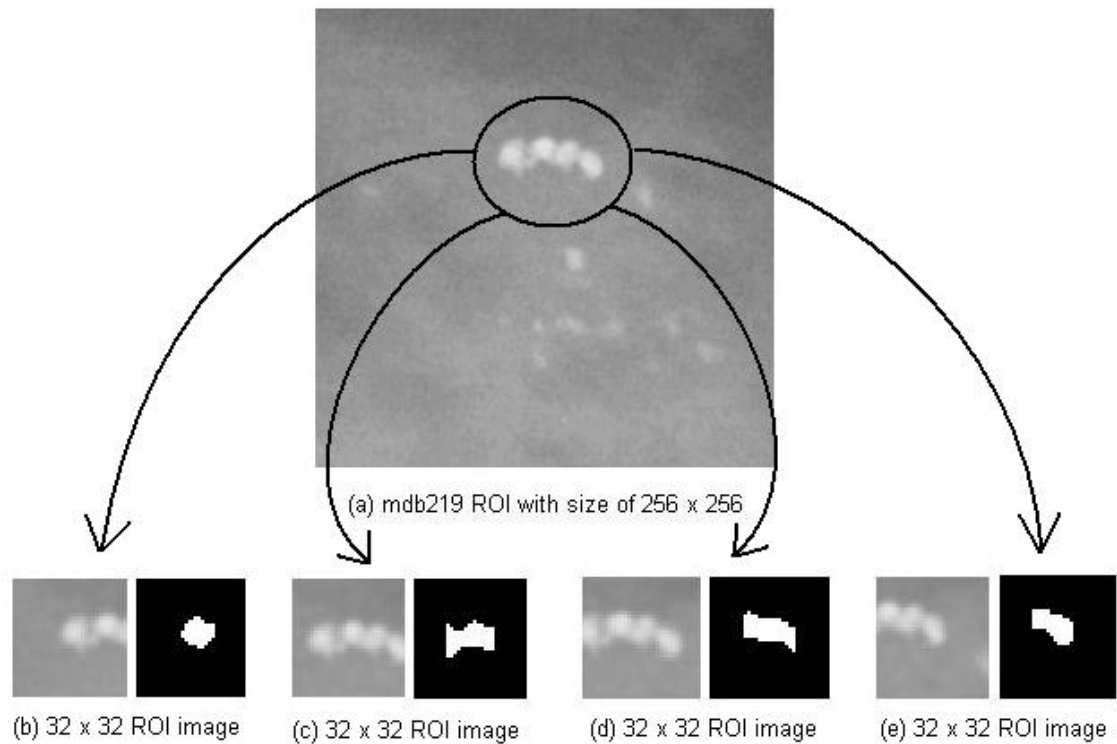
Figure 3.17 The original image of a cluster of microcalcifications from mammogram image mdb219 in (a). individual microcalcifications centred in the images (b), (c), (d) and (e) after cropping into size32 × 32 pixels.

The performance of the thresholding technique has been evaluated in Table 1 based on the percentage of suspicious objects segmented within a region of interest. This evaluation is done between the square filter and the circular filter using different threshold values that have been tested on a variety of ROI image sizes. The results shown in Table 1 demonstrate an improvement using a circular filter shape rather than using a square filter under different thresholding values. In addition, choosing the threshold value of 10 matches the size of the (i.e. 1.5 pixels of the inner window and 11 pixels for the outer window) filter better than other threshold values.

Table 3.1 Thresholding percentage of different thresholding values between square and circle filters

Threshold Value	Percentage of detected objects using square filters	Percentage of detected objects using circle filters
6	0.0489	0.0635
7	0.0310	0.0366
8	0.0211	0.0297
9	0.0135	0.0204
10	0.0102	0.0157

3.4. Thresholding to 8-bit Images

In this section, the same criterion of thresholding has been applied using Eq. (3.1) for both filter shapes (i.e. square and circle). However, the output image this time is an 8-bit grey scale image. The thresholding technique in this experiment is going to locate suspicious objects, keeping the original grey scale colour of the microcalcification or any other suspicious objects and removing the background (i.e. converting the surrounding breast tissue to black colour). The following Figures 3.18 and 3.19 are an illustration of different ROI images showing the original image after applying the thresholding technique using different thresholding values.

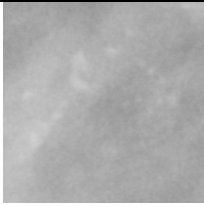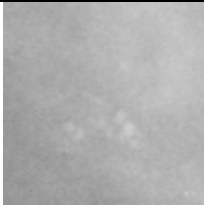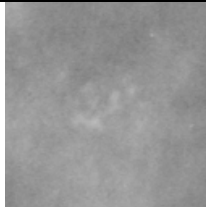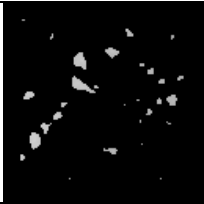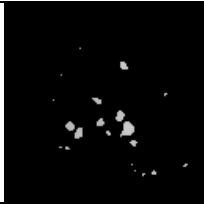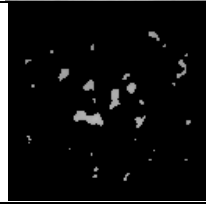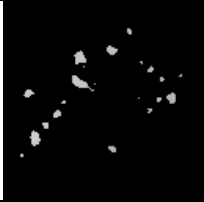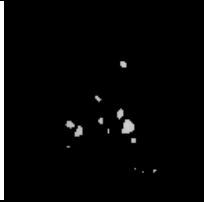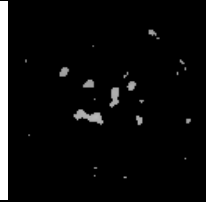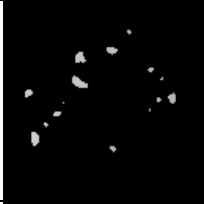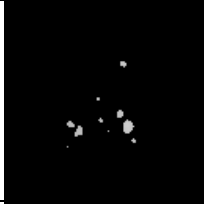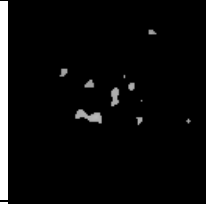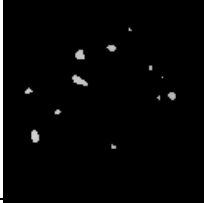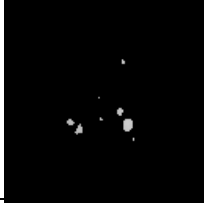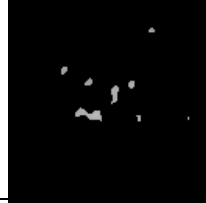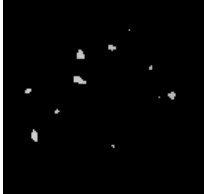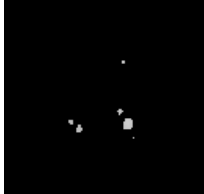**Figure 3.18** Applying circular filter using 1.5 pixels for inner window and 11 pixels for outer window using different threshold values
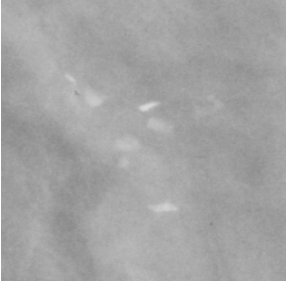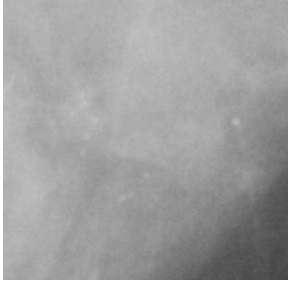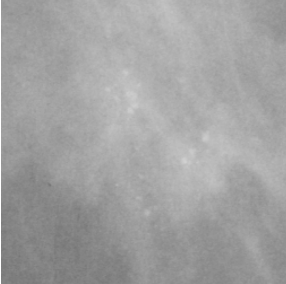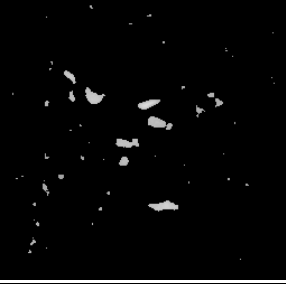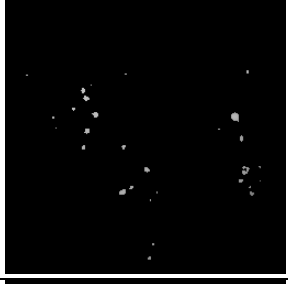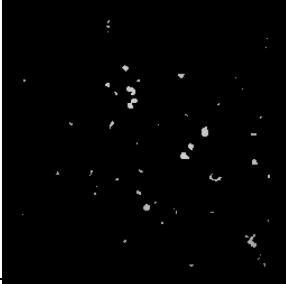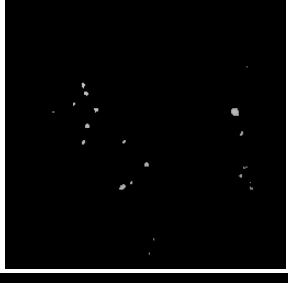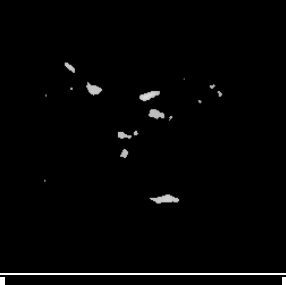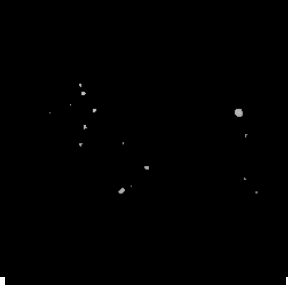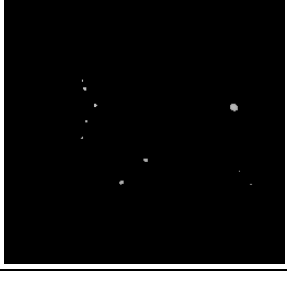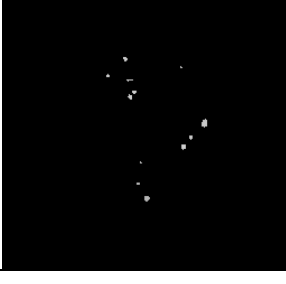
Figure 3.19 Applying circular filter using 1.5 pixels for inner window and 11 pixels for outer window using different threshold values

3.5. Summary

The segmentation stage is implemented using a simple but effective method for detecting potential microcalcifications and other suspicious objects in breast tissue taking account of variations in tissue density between women and the low contrast between the abnormal and normal breast tissues. This method has been applied on:

- Full mammogram images of various mammogram sizes (i.e. small, medium, large and ex-large);

- A dataset of ROI images that represent clusters of microcalcifications with different sizes (i.e. 128×128, 256×256, 512×512 and 1024×1024);

- A dataset of ROI images that represent individual microcalcifications with images of size 32×32.

The results were slightly different depending on the threshold filter shape as shown in section 3.3.2 in Table 1. The circular filter shape has a higher percentage of locating microcalcifications within an image than using the square filter shape and that applies also on different thresholding values. The thresholding technique is applied to generate two different output images the first is binary ROI images and the second is 8-bit grey scale ROI images. Testing these filters on different images that focus on certain areas as in ROI images, rather than on larger areas like full mammogram made a slight difference. For instance, using circular filter rather than square shape did suit the shape of microcalcifications by either covering a full individual microcalcification or by detecting its peak; while the square filter what it did is partially cover an individual microcalcification, but still detected the microcalcification. Moreover, the number of false positives will be reduced if the detection task will be focused only within a region of interest instead of dealing with

a whole mammogram. Furthermore, when applying the filter on 32 × 32 images of individual microcalcifications the filter should either detect the abnormality or miss it; this gives the opportunity to figure out which filter parameter needs to be tuned quickly to be able to detect a microcalcification in that area, if it is available. However, when applied on full mammogram images these filters can pick up suspicious objects that are similar to microcalcifications in shapes, sizes or intensities (such as milk ducts or blood veins). The following chapter, feature extraction, will help by identifying abnormalities using certain features that could distinguish them from other objects.

References

1. Fu, J.C., Lee, S.K., Wong, S.T.C., Wong, J.Y., Wang, A.H., and Wu, H.K., *Image segmentation feature selection and pattern classification for mammographic microcalcifications.* Computerized Medical Imaging and Graphics, 2005. **29**(6): p. 419-429.

2. Wirth, M.A. and Stapinski, A., *Segmentation of the breast region in mammograms using active contours.* Visual Communications and Image Processing, 2003. **5150**: p. 1995-2006.

3. Lefebvre, F., Benali, H., Gilles, R., Kahn, E., and DiPaola, R., *A fractal approach to the segmentation of microcalcifications in digital mammograms.* Medical Physics, 1995. **22**(4): p. 381-390.

4. Campanini, R., Angelini, E., Iampieri, E., Lanconelli, N., Masotti, M., Roffilli, M., Schiaratura, O., and Zanoni, M., *A fast algorithm for intra-breast segmentation of digital mammograms for CAD systems*, in *7th International Workshop on Digital Mammography.* 2004: Durham, North Carolina, USA.

5. Gavrielides, M.A., Lo, J.Y., Vargas-Voracek, R., and Floyd, C.E., *Segmentation of suspicious clustered microcalcifications in mammograms.* Medical physics, 2000. **27**(1): p. 13-22.

6. AbuBaker, A.A., *Automatic Detection of Breast Cancer Microcalcifications in Digitized X-ray Mammograms.* Electronic Imaging and Media Communications. Ph.D. 2008, Bradford: University of Bradford.

7. AbuBaker, A., Qahwaji, R., and Ipson, S., *Knowledge-based Approach to the Automatic Detection of Microcalcifications in Mammogram Images.* Medical Image Analysis, Elsevier, 2007.

8. Shapiro, L.G. and Stockman, G.C., *Computer Vision.* 2001: Prentice Hall. 608.

9. Kom, G., Tiedeu, A., and Tiedeu, M., *Automated detection of masses in mammograms by local adaptive thresholding.* Computers in Biology and Medicine, 2007. **37**(1): p. 37-48.

Chapter 4

Feature Extraction using Wavelet Transforms

4.1. Introduction

This chapter discusses and demonstrates how segments of an image be represented by features. Feature extraction is an essential process in the research field of digital image interpretation, as it provides condensed information representing much larger multi-dimensional data. Feature extraction in mammography is a specific application where the features are the key to identifying abnormalities such as microcalcifications and masses. The features extracted are utilized in image classification, which is the subject of Chapter 5.

In this chapter, wavelet decomposition is introduced as the main method for feature generation. Due to the nature of microcalcifications, which appear as small bright dots within a mammogram, they also appear as point discontinuities for the wavelet transform [1]. This makes the wavelet transform appropriate to detect microcalcifications and for feature generation as it is argued that wavelets have finite square supports and are best in capturing point discontinuities and not edges [2].

Moreover, applying the discrete wavelet transform (DWT) would be more appropriate than using the continuous wavelet transform (CWT); since the CWT is time consuming and needs a lot of computation, calculating all points on the spatial

domain signal. On the other hand, DWT would take samples from the signal and that would take less time and computation. Additionally, wavelet transform, when applied, will save the location of all pixels within the image that might be useful for image reconstructing.

Furthermore, in this research the use of wavelet decomposition to generate features combined with support vector machines for classifications produced satisfying results as it will be shown in the following chapter. There are many different types of wavelet transforms that can be applied such as Haar, Daubechies, Biorthogonal, Coiflets, Discrete Meyer 'dMey', and Symlets as well as many different ways of defining features. Here the largest approximation coefficients are used as features and different numbers of features are tested either by extracting (80 and 100), or by extracting the largest 100 and using a reduction method to reduce the number to 10 coefficients.

The following section discusses the discrete wavelet transform and the main concepts that are useful for this type of research dealing mainly with binary images. Then, in Section 3 the minimum Redundancy Maximum Relevance (mRMR) reduction method is introduced and applied to wavelet features. Finally, Section 4 describes the implementation of the wavelet decomposition steps and how it is linked to the classification stage described in Chapter 5.

4.2.   Discrete Wavelet Transform

The discrete wavelet transform (DWT) is a hierarchical sub-band technique, often used in multi-resolution pattern recognition [3], which was employed here to extract features from the binary images produced by the segmentation process described in Chapter 3. The basic steps of the 2-D wavelet decomposition algorithm are shown in

Figure 4.1. One application of the transform proceeds as follows. A low-pass and related high-pass filter are applied to each row (and column) of the input image. Each filtered row (column) is sub-sampled by a factor 2, throwing away half the filtered data to arrive at the same number of values as in the original row (column). The low-pass samples are grouped together and the high-pass samples are grouped together. The process can be repeated on the low-pass filtered samples to provide transformed data corresponding to a lower resolution. Each discrete wavelet transform has its own low-pass and high-pass filter pair and the process can be inverted to proceed from the transformed data back to the original data.
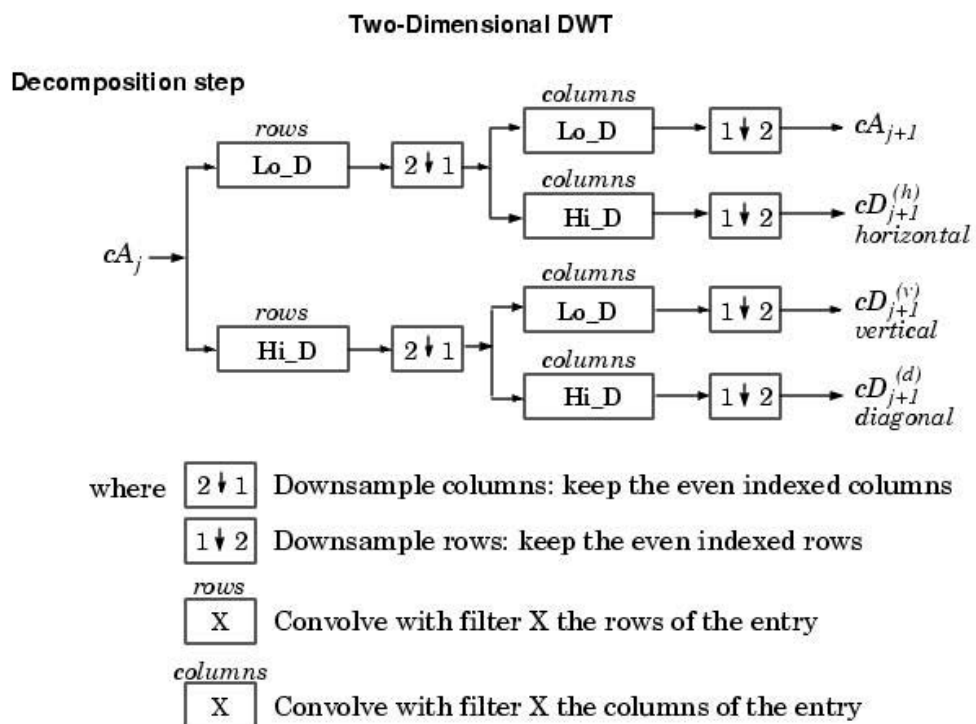
Figure 4.1 Two dimensional discrete wavelet transform algorithm.

When the DWT is applied, it generates low-pass and high-pass sub-bands that contain many coefficients representing different aspects of the image. The wavelet

coefficients represent the characteristics of the signal at different resolutions (scales) and positions according to the number (level) of times the wavelet is applied [4].

4.2.1. Wavelet Coefficients

The Wavelet coefficients are divided into low (L) frequency approximation-coefficients and high (H) frequency detail-coefficients. The high frequency coefficients are further divided into detail sub-bands: vertical (LH), horizontal (HL), and diagonal (HH) coefficients. The low frequency (LL) approximation-coefficients provide a reduced resolution representation of the original image which can be transformed again according to the wavelet level applied. Applying wavelet decomposition to an image will produce an approximation matrix that is a quarter of the original area of an image.

The decomposition of an image into sub-bands by two applications of the DWT is illustrated in Figure 4.2. Each application filters the image in horizontal and vertical directions creating the four wavelet sub-bands [5] shown in Figure 4.2. These are labelled as follows:

- Sub-band LL1 represents the horizontal and vertical low frequency components of the image, known as the approximation coefficients. In Figure 4.2 the coefficients in this band are transformed again and replaced by four corresponding level 2 sub-band coefficients.

- Sub-band HH1 represents the horizontal and vertical high frequency components of the image, also known as diagonal coefficients.

- Sub-band LH1 represents the horizontal low and vertical high frequency components, known as vertical coefficients.

- Sub-band HL1 represents the horizontal high and vertical low frequency components, known as horizontal coefficients.
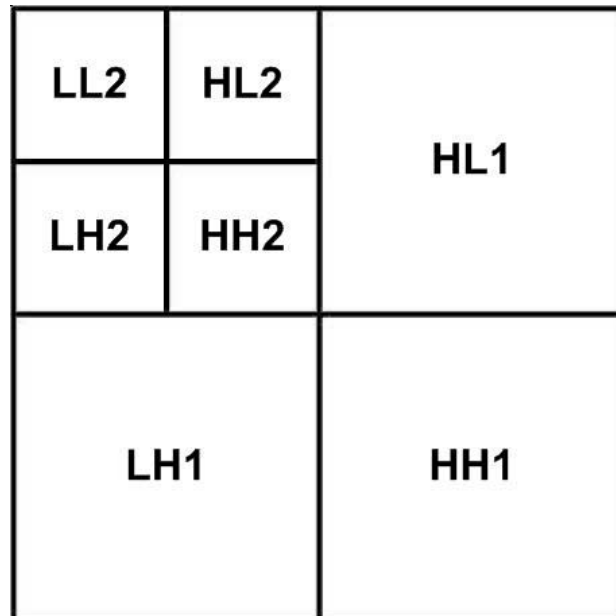
Figure 4.2 Simple decomposition map from the wavelet transform level two

Different wavelet transforms can be applied, including Haar, Daubechies, Biorthogonal, Coiflets, dMay, and Symlets etc. Each has its own characteristics. The MATLAB wavelet toolbox has been used in this study as it provides a variety of functions and wavelet types as well as other functions that are useful for this kind of application.

Figure 4.3 shows an example of applying the Haar wavelet, which is the simplest wavelet available, to a grey scale ROI image. By inspecting the resulting images it is clear that the high frequency coefficients are not focused on the microcalcifications cluster, instead the detail sub-bands appears like noisy images. Although not apparent from this figure, the approximation coefficients enhance the brightness of the abnormalities.
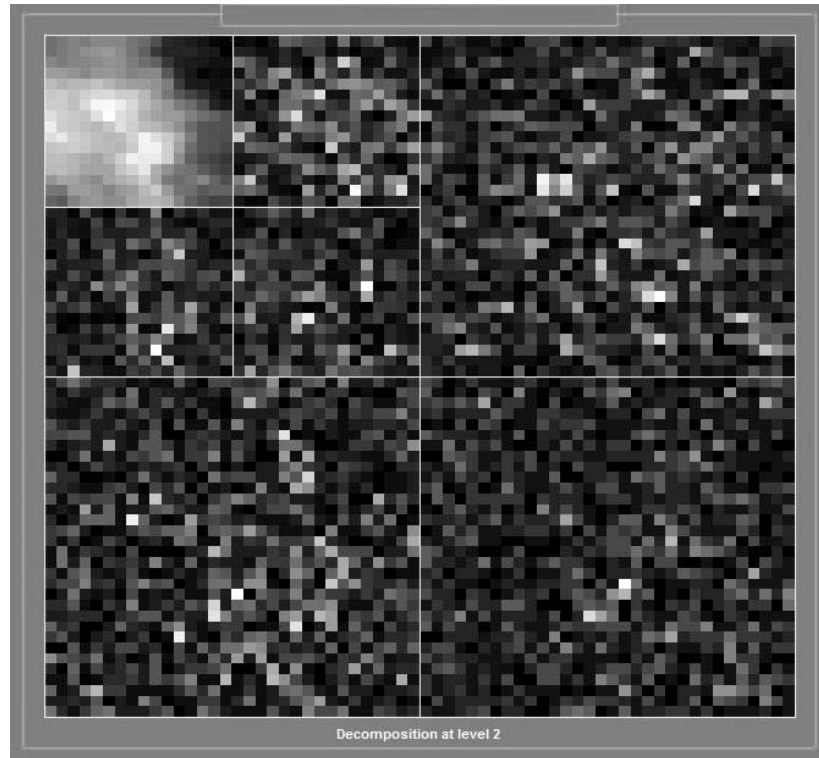
Figure 4.3 Haar wavelet decomposition at level 2 on grey scale region of interest; first view

Figure 4.3 shows the default view of wavelet decomposition with the features extracted from the top left corner, which is the low frequency image from the second level of decomposition. The results are shown more clearly by changing the default view to the alternative view, Figure 4.4, that shows all the images from each level separately and at the same size. This provides a better view of the differences between levels of decomposition especially when looking at the low frequency image that produces the approximation coefficients for our features. The figure shows the original image at the top and below it are the approximations from level 1 and level 2 of decomposition showing microcalcifications in a larger area than from the original image.
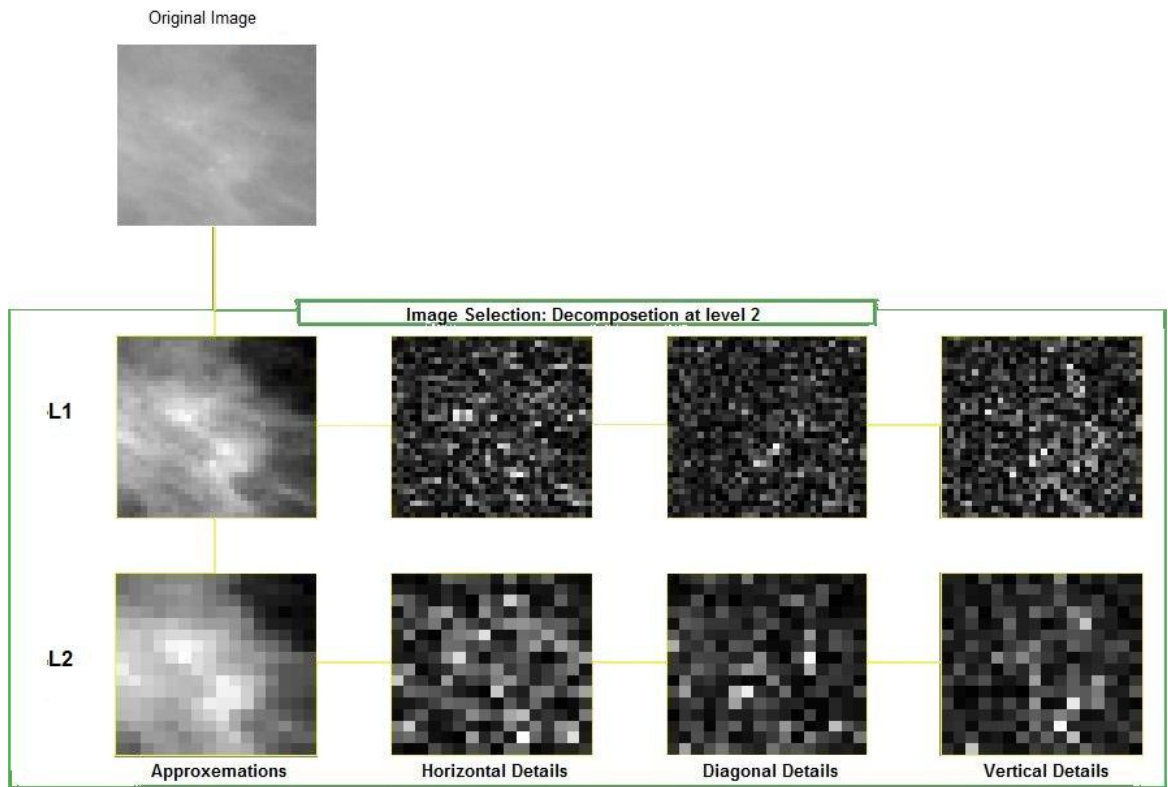
Figure 4.4 Haar wavelet decomposition at level 2 on grey region of interest; second view

4.2.2. Feature Extraction from ROI Images

This part of the experimental work takes the segmented ROI images (i.e. the resultant binary ROI image and 8-bit grey scale image) produced by the previous stage for analysis by the extraction of unique features. The previous figures showing wavelet examples are only illustrations of the basic characteristics. The use of segmented ROI images (i.e. binary and 8-bit grey scale) was found to be more successful than using original ROI images for extracting features. The examples in the figures below illustrate the application of different wavelet decomposition types on different sizes of images. Figure 4.5 to 4.7 show the application of Daubechies-2, Haar and dMey wavelets level 1 and 2 on a region of size 32×32. Moreover, Figures 4.8 to 4.10 show the application of Haar, Daubechies order 2 and dMey wavelets from level 1 and 2 on regions of sizes 128×128, 256×256 and 512×512. These figures show

level one and level two decompositions; the first image to the left in each row is the approximation sub-band and the rest are the high frequency sub-bands.
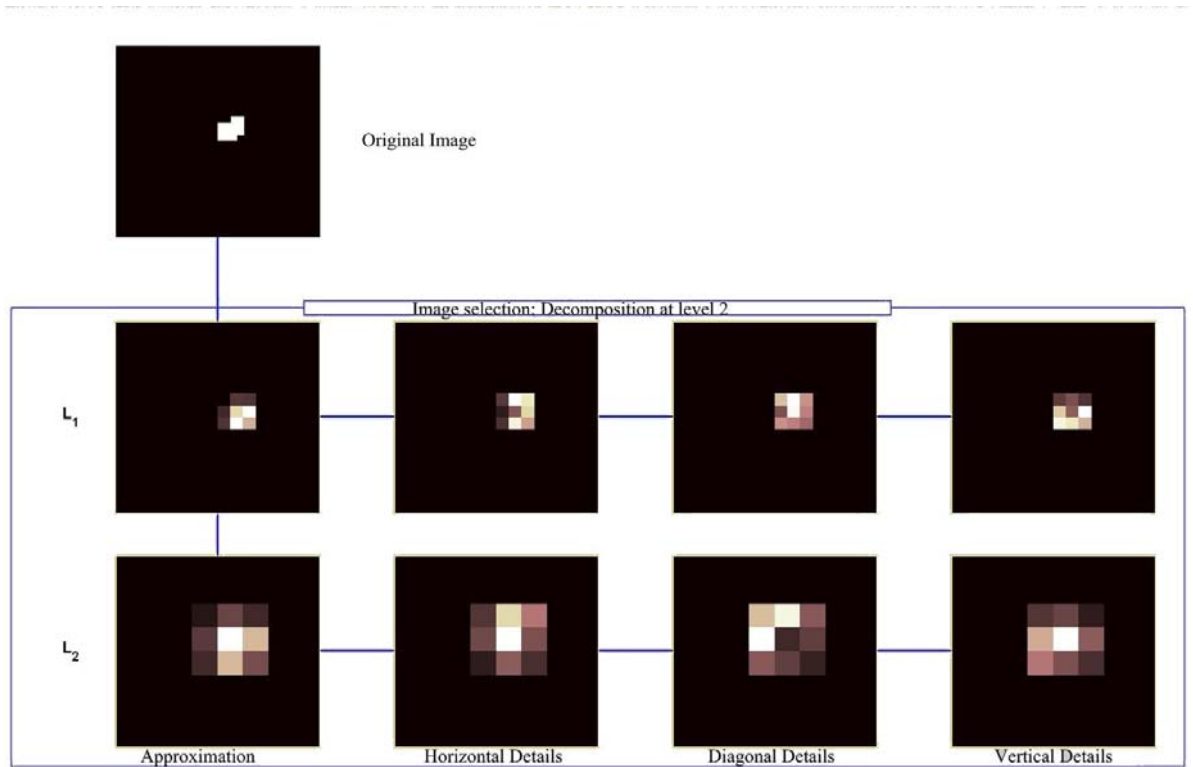
Figure 4.5 Wavelet decomposition results from applying DB-2 wavelet at levels 1 and level 2 to a 32 × 32 region of interest
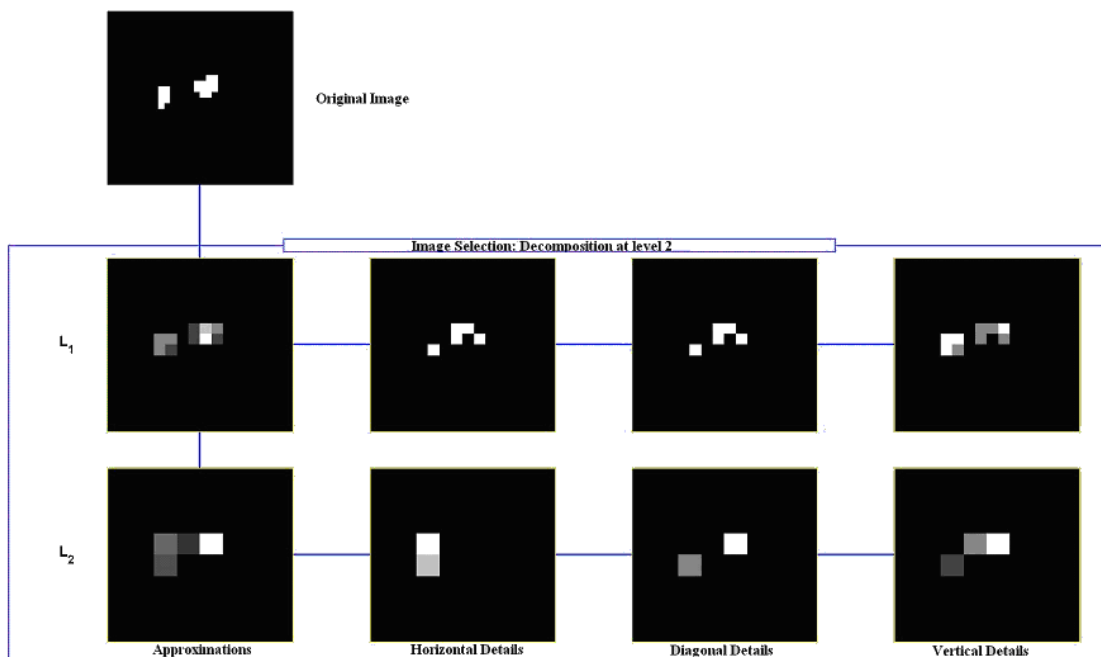
Figure 4.6 Wavelet decomposition results from applying Haar wavelet at levels 1 and level 2 to a 32×32 region of interest
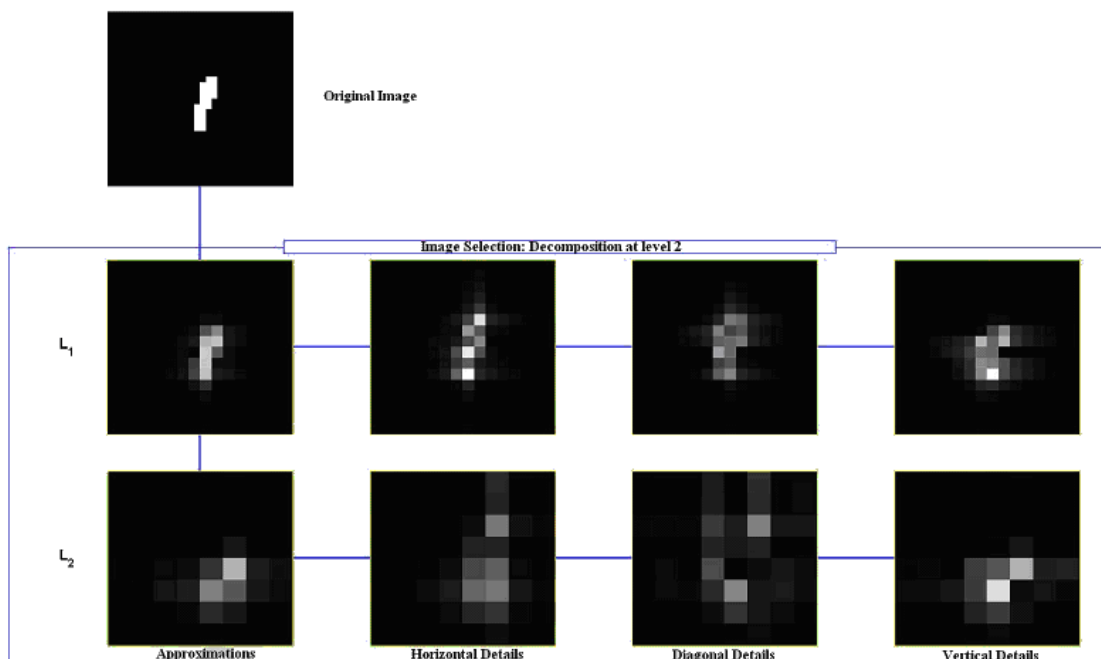
Figure 4.7 Wavelet decomposition results from applying dMey wavelet at levels 1 and level 2 to a 32×32 region of interest
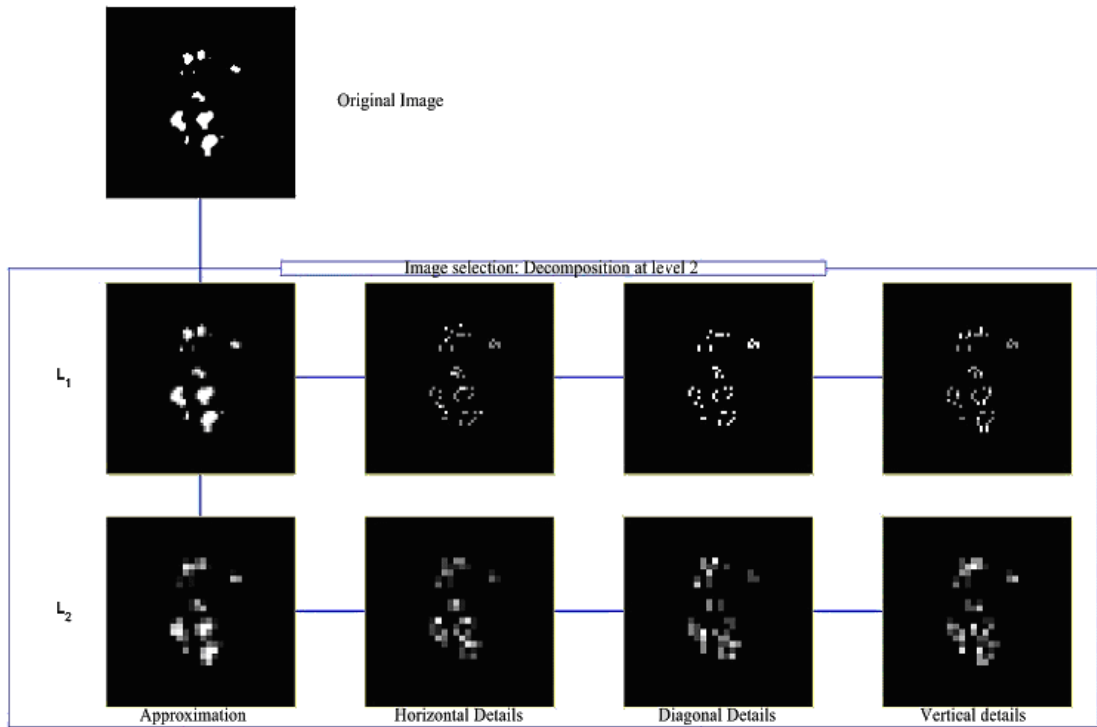
Figure 4.8 Wavelet decomposition results from applying Haar wavelet at levels 1 and level 2 to a 128 × 128 region of interest
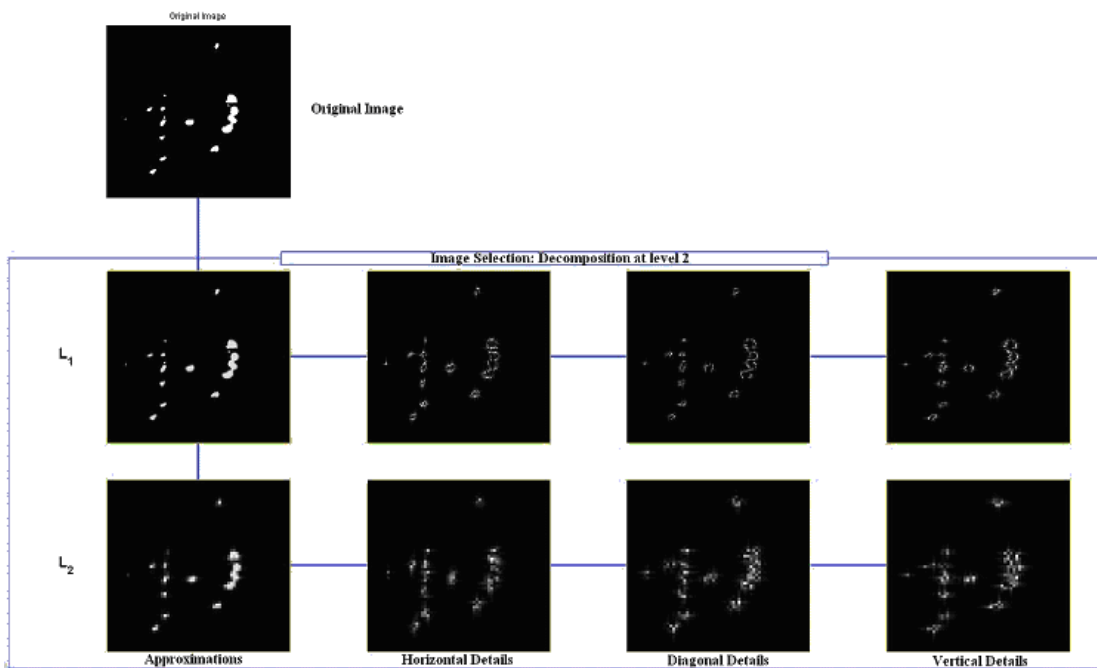
Figure 4.9 Wavelet decomposition results from applying dMey wavelet at levels 1 and level 2 to a 256 × 256 region of interest
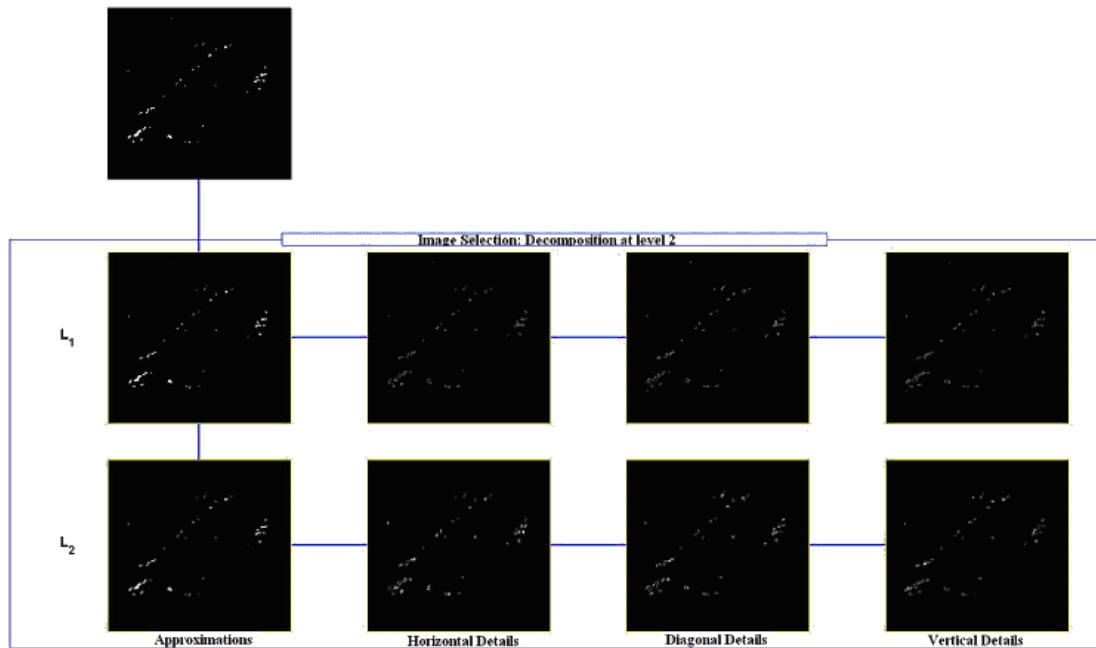
Figure 4.10 Wavelet decomposition results from applying DB-2 wavelet at levels 1 and
level 2 to a 512×512 region of interest

During this study, the approximation coefficients have been used as the target
coefficients from which to extract features. The selection of the low frequency
coefficients is suggested by Ferreira and Borges in [6] that used the mini-MIAS
database as its source. In that study, feature extraction is made on original ROI grey
scale images using two types of wavelet transform: the Haar wavelet and Daubechies
wavelet (Db4). However, the use of approximation coefficients in these experiments
is carried out on segmented binary and 8-bit grey scale images using the largest 100
approximation coefficients as in [6] in conjunction with investigating further types of
wavelet transform and different levels of decomposition. Also the use of different
number of features, such as largest 80 coefficients and largest 10 coefficients, was
investigated.

Wavelet decomposition can be done to any level, up to a maximum set by the size of
the image, depending on the nature of the application it is used for and what data

needs to be extracted. The diagram in Figure 4.11 below shows the division of wavelet coefficients from level three of decomposition. In the first level of wavelet decomposition the original image will generate high frequency coefficients (cD1) and low frequency coefficients (cA1). Then level two of decomposition will be applied on cA1, which represent a lower resolution of the original image, to generate cA2 and cD2. The same process will be applied on cA2 to generate cA3 and cD3. And so on as long as the application requires.
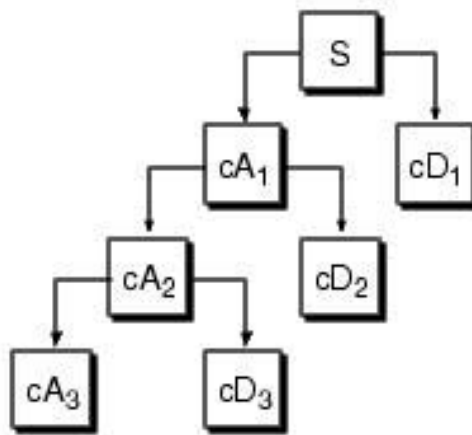
Figure 4.11 The coefficients resulting from applying wavelet decomposition of three levels

The wavelet approximation coefficients were found useful in this work when they were combined with support vector machines, as this combination produced satisfying classification accuracy, as shown in Chapter 5.

4.3. Minimum Redundancy Maximum Relevance

After the initial feature generation, another experiment was conducted to investigate if it is possible to reduce the largest 100 wavelet coefficients to a smaller number of useful features. This reduction was performed using the minimum Redundancy Maximum Relevance (mRMR) approach and software that is available online [7]. This software package is basically a feature selection and classifier package used for pattern classification. During this experiment the mRMR approach was used to reduce the 100 selected largest coefficients to 10 features. This is done to reduce the number of features that are fed to the classifier, as this will decrease the amount of the computation time for classification.

The mRMR procedure essentially starts searching for features that suit the criterion of maximal relevance using the mean value of all mutual information values between individual features and their classes. Then the minimal redundancy criterion is used because the feature dependencies can be very large, so only mutual features will be selected. Two types of mutual information schemes can be applied, mutual information difference (MID) and mutual information quotient (MIQ).

The features for each region are presented as a row in the file input to mRMR and specified as either normal (0.1) or abnormal (0.9). The data in the input format can be one of two types either categorized, in terms of discrete category states or continuous in terms of numerical values. If it is continuous then the data is discretized using two thresholds

$$Threshold = mean \pm alpha \times standard\ deviation \qquad (eq.\ 4.1)$$

where alpha can be either 1 or 2 or 0 or 0.5. This choice affects the actual features selected. The outputs are the features that satisfy the mRMR condition (eq. 4.1) and are ordered according to their entropy score.

4.4.   Practical Implementation of Wavelet Analysis

First of all, the discrete wavelet transform is applied to the segmented binary images cropped using the algorithm in [8]. Transform coefficients are used as extracted features from both normal and abnormal regions.

The wavelet toolbox in MATLAB provides several functions [9] to complete this task. These functions require several inputs and these include a matrix which is the image data, the level of decomposition required, and the wavelet name.

The first step in the process is to collect all the image names in a text file. This file is to be read by a MATLAB script which calls the wavelet decomposition code which processes all the images in sequence to generate the transform coefficients. Then a small coded loop is used to extract the largest 100 coefficients in a vector that contains the data for an individual image.

To generate a reduced number of coefficients out of the largest 100 coefficients the MATLAB code stores the largest 100 coefficients in a file format that is accepted as an input by the mRMR application. Then by applying the threshold condition mentioned in (eq. 4.1) this reduces the largest 100 coefficients to 10 coefficients as another set of features for the next stage of the classification. Each set of features from different wavelet types or from different numbers of features are then tested to see how useful they are in a classification system.

4.5. Summary

Feature extraction is an important part of this study. To analyse and study the abnormality, in this case microcalcifications, it is necessary to find unique features that can distinguish the abnormality from any other surroundings or artefacts that have similar shapes or intensities. Therefore, many experiments were carried out at this stage to investigate the following:

- Wavelet decomposition types including, the Haar wavelet, Daubechies wavelet, Biorthogonal wavelet, Coifielts wavelet, Discrete Meyer "dMay" wavelet and Symlets wavelet.

- Wavelet decomposition levels including the first two levels of wavelet decomposition on all six wavelets types.

- Different numbers of approximation coefficients have been tested including the largest 10, 80 and 100 coefficients. In addition mRMR was used to reduce the largest 100 coefficients to only 10 features.

- Applying the wavelet decomposition on segmented binary and 8-bit ROI images.

However, after combining these features with support vector machine, at the next stage, it was found that the largest 100 approximation coefficients produced the best results in the classification stage experiment. The following chapter on the classification stage indicates how these features were evaluated on radial bases function (RBF) and support vector machine (SVM).

References

1. Sampat, M.P., Markey, M.K., and Bovik, A.C., *Computer-aided detection and diagnosis in mammography*, in *Handbook of Image and Video Processing*, 2nd ed. 2005, New York: Academic Press. pp. 1195-1217.

2. Candès, E.J. and Donoho, D.L., *Ridgelets: a key to higher-dimensional intermittency?* Philosophical Transactions of the Royal Society A Mathematical, Physical & Engineering Sciences, 1999. **357**(1760): pp. 2495-2509.

3. Ferreira, C.B. and Borges, D.L., *Automated mammogram classification using a multiresolution pattern recognition approach.* Proc. XIV Brazilian Symposium on Computer Graphics and Image Processing, 2001: pp. pp. 76-83.

4. Kaplan, I. *Wavelet and signal processing.* 2003 [cited 2008 March]; Available from: http://www.bearcave.com/misl/misl_tech/wavelets/index.html.

5. EPSILON LABS. *Electronic Product Design Service* [cited 2009 May]; Available from: http://www.epsilonlabs.com/Wavelets.html.

6. Ferreira, C.B.R. and Borges, D.L., *Analysis of mammogram classification using a wavelet transform decomposition.* Pattern Recognition Letters, 2003. **24**(7): pp. 973-982.

7. Peng, H. *minimum Redundancy Maximum Relevance Feature Selection.* [cited 2008 March]; Available from: http://penglab.janelia.org/proj/mRMR/.

8. AbuBaker, A.A., *Automatic Detection of Breast Cancer Microcalcifications in Digitized X-ray Mammograms*. PhD. 2008: University of Bradford.

9. Gonzalez, R.C., Woods, R.E., and Eddins, S.L., *Digital Image Processing Using MATLAB*. 1st ed. 2004: Prentice Hall

Chapter 5

Machine Learning and Microcalcification Classification

5.1. Introduction

Machine learning is a part of the artificial intelligence field where machines or computers are developed to imitate the human ability to think by a process of training (or related technique) and separate testing. There are two basic types of machine learning, supervised and unsupervised techniques. Different fields of studies have different learning needs; applying a supervised learning technique means some targets classifications are already known, on the other hand, applying an unsupervised learning technique means that target classifications are not available and these need to be predicted based on the input vector(s) to the system. Both techniques require extensive training where for supervised techniques the inputs or the machine parameters need to be tuned to match the target, while for unsupervised training machine tuning will be made to achieve logical targets.

In the current research the supervised learning technique was selected for the classification task as target class labels (either normal or abnormal) are already known. Furthermore, digital mammography systems or computer aided detection/diagnosis

systems (CAD systems) are basically considered as a source of second opinions for radiologists. Therefore, suggestions made by a digital diagnosis system are studied by a radiologist and double checked for any abnormalities that were missed by the radiologist. Having a classification stage in this study is essential; since machine learning has the ability to distinguish between regions containing microcalcifications or other suspicious objects and regions that contain normal breast tissue. This process assists radiologists in the diagnosis procedure, since mammography needs a high level of experience in diagnosis which in this medical case is radiologists

Machine learning in this research is focused on classifying region of interest images that are cropped manually into two ROI sets; clusters of microcalcifications and individual microcalcifications. The classification training will look into regions that contain abnormalities, specifically cases that contain microcalcifications, which are extracted from mammogram images in the MIAS database. Moreover, features that are extracted and using the discrete wavelet transform are fed to machine learning experiments for classification purposes. The main purpose of this classification is to distinguish between normal breast tissue and breast tissue that is infected with an abnormality of a microcalcifications type. In addition, any suspicious objects that have similar characteristics will be also diagnosed.

In this research, the Support Vector Machine (SVM) and the Radial Basis Function Network (RBFN) have been tested on the feature data extracted from regions of interest of mammogram images. The two approaches, SVM and RBFN, are different in concept but they are both types of machine learning algorithms capable of providing data classification.

The following sections provide more details about Support Vector Machines and Radial Basis Function Networks. In addition, experiments and their results are presented.

5.2. Classifiers

5.2.1. Support Vector Machines

Support Vector Machines (SVM) are a supervised learning technique that can be used for classification and regression [1]. SVMs have a firm statistical foundation and are guaranteed to converge to a global minimum during training. They are also considered to have better generalisation capabilities than neural networks [2]. SVMs were developed by Vapnik in [3] based on statistical learning theory. SVM is known to be an excellent tool for binary classification problems, similar to the one here, by seeking the optimal separating hyperplane that provides efficient separation of the data and maximises the margin. In other words, SVM takes the closest vectors from both classes, assuming they are linearly separable, and maximises the distance between them by a hyperplane. On the other hand, if the data are not linearly separable, using kernel functions, SVM will map the data into a higher dimensional feature space where the data can become linearly separable. More information on SVMs can be found in [4] and [3]. Support vector machines are applied in the experiments described in the following sections to evaluate the quality of different feature extraction sets and feature reduction for classification purposes. In this work, there are only two output class labels: normal and abnormal. Hence, the classification is binary.

5.2.2. Radial basis function (RBF)

The RBF Network is a powerful interpolation technique that can be efficiently applied in multidimensional space. The RBFN approach to classification is based on curve fitting. Learning is achieved when a multidimensional surface is found that can provide optimum separation of multidimensional training data. In general, the RBFN can model continuous functions with reasonable accuracy. The RBFN are a set of functions provided by the hidden nodes that constitute an arbitrary "basis" for the input patterns[4]. One major advantage of using the RBFN is that the training is usually simpler and shorter compared to other neural networks. On the other hand it requires greater computation and storage for input classification after the training [5].

The RBFN, as illustrated in Figure 5.1, applies a mixture of supervised and unsupervised learning modes. The layer from input nodes to hidden nodes is unsupervised, while supervised learning exists in the layer from hidden nodes to output nodes. A non linear transformation exists from input to hidden space, while a linear transformation exists from the hidden to the output space [6]. More information on the theory and implementation of RBFNs can be found in [4] and [5].
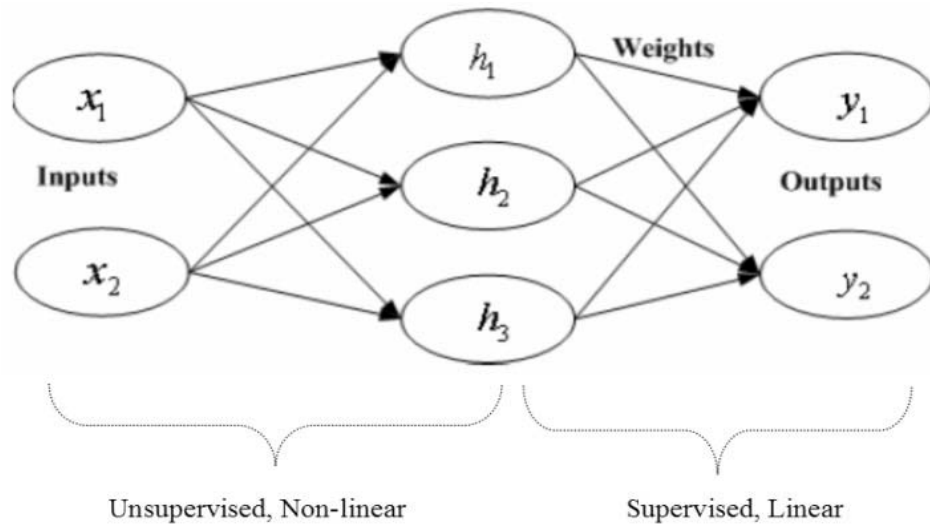
Figure 5.1 RBF network with 2 input and 2 output nodes

5.3. Implementation and Evaluation

5.3.1. Jack-Knife Technique

To achieve reliable results, one must follow an appropriate technique for training and testing. Therefore, the SVM training and testing was carried out based on the statistical Jack-Knife technique [7], which divides the input data into two groups. There is a training group which consists of 80% of the samples, randomly selected, and the remaining 20% which forms the testing group. This is done to allow accurate statistical evaluation of the performance of the classifier, when it is applied on a limited number of samples. Thus, the number of training samples from the dataset consisting of individual microcalcification ROIs is 352 samples, while 88 samples were used for testing the classifier. Moreover, from the second dataset, which contains 25 cluster of microcalcification ROIs, 20 samples are selected for training and 5 for testing; and likewise for the third dataset from the mini-MIAS database.

5.3.2. RBF Implementation

Two sets of features from cropped regions of interest were fed to an RBFN, the largest 100 features and the 10 mRMR reduced features generated from Haar and DB2 wavelet level 1 approximation. The results were not satisfactory as the accuracy using the largest 100 features reached 58.27% and the accuracy using the 10 mRMR features reached 49.8%. For this reason and the better performance of SVM, trials using the RBFN were not taken further

5.3.3. SVM Implementation

After the wavelet features are extracted from cropped regions of interest they are stored in a text file format that matches the format required for SVM input. This text file contains the input features of a set of images and the corresponding output class labels, normal and abnormal. The format is illustrated in Figure 5.2 where each row is a feature vector and at the end is the corresponding output class, either 0.1 or 0.9, representing normal or abnormal classes respectively.

```
28 280.08 277.86 275.08 269.34 263.75 0.9
37 11.766 11.473 11.45 11.433 11.418 0.9
96.26 176.37 147.22 146.64 142.09 136.11 0.9
 0.5924 0.5377 0.4937 0.4469 0.4037 0.3566 0.9
12 60.976 57.074 55.714 55.478 55.443 54.136 0.9
909 0.1804 0.1738 0.1594 0.154 0.1526 0.1404 0.9
4.0842 3.8213 3.798 3.6576 3.5444 3.4424 0.9
717 1.5284 1.4825 1.3626 1.2665 1.1241 0.9

7 20.088 19.468 19.149 18.876 0.9
.0236 0.023 0.0223 0.0184 0.0155 0.0148 0.9
 3.1609 3.1466 3.0701 3.0437 3.0089 2.8506 0.9
2 0.0502 0.0476 0.0406 0.032 0.0242 0.0233 0.9
4616 1.3895 1.28 1.223 1.2034 1.1772 0.9
0298 0.0217 0.0207 0.0198 0.0194 0.0194 0.9
05 0.0004 0.0004 0.0002 0.0002 0 0 0.9
0.0001 0.0001 0.0001 0 0 0 0.9
0645 0.0598 0.0594 0.0589 0.0576 0.0491 0.9
 12.19 11.963 11.554 11.306 10.657 0.9
.0157 0.0142 0.0112 0.0111 0.011 0.0106 0.1

279 1.8875 1.7814 1.7286 1.6887 1.6316 1.541 0.1
.0604 0.0567 0.0525 0.0523 0.0508 0.0454 0.1
361 0.8064 0.6483 0.6324 0.6324 0.1
0138 0.0129 0.0128 0.0125 0.0115 0.0099 0.1
41 0.2041 0.2022 0.1857 0.1857 0.1814 0.169 0.1

 0.0016 0.001 0.001 0.001 0.0008 0.0007 0.1
```

Figure 5.2 Input features and output class labels which are ringed in green or red

These features vectors, illustrated in Figure 5.2, are extracted and gathered from the approximation coefficients of wavelet decomposition, this has been explained in Chapter 4 section 4.4. Basically, after applying wavelet decomposition, the largest numbers of features are extracted for individual image to form a vector. This includes normal images and images that contain microcalcifications. Then all vectors are collected in a text file from all samples processed and adding a label to each vector.

The SVM learning algorithm used in this work employs the ANOVA kernel. The Anova kernel technique was adopted because it produced the best classification performance, in a different area of research [2, 8], compared to other types of kernels such as the dot, polynomial, neural and radial kernels. The Anova kernel, which is shown in equation (eq. 5.1), has two parameters, the gamma (γ) parameter and the exponential degree (d) parameter. These two parameters control the shape of the kernel.

$$k(x, y) = \left\{ \sum_i \exp\left[-\gamma(x_i - y_i) \right] \right\}^d \qquad \text{(eq. 5.1)}$$

An important part of the machine learning process is optimization of the SVM. This is to determine the topology and parameters for the learning algorithm that produce the best performance. In this work, extensive experiments were carried out to find the optimum degree and gamma values. Thus, the gamma value was changed from 1 to 10 in steps of 1 and for each gamma value the degree values 2, 3 and 4 were used. Hence, a total of 30 experiments were carried out, for every set of wavelet coefficients features used. For each experiment, the Jack-Knife technique was implemented ten times and the average value for these ten iterations was found and associated with the experiment.

There were seven output values generated for every experiment namely true positive (TP), false positive (FP), true negative (TN), false negative (FN), accuracy, sensitivity and specificity. When a positive object is detected and classified as positive then this is called a true positive. However if this object is classified as negative then this is false negative. On the other hand, when a negative object is detected and classified as positive then this is called a false positive, and when it is classified as negative then this is a true negative. Sensitivity is the percentage of patients with disease who test positive and is calculated as follows:

$$Sensitivity = \frac{TP}{(TP + FN)} \qquad \text{(eq. 5.2)}$$

Specificity, on the other hand, is the percentage of patients without disease who test negative and is calculated as follows:

$$Specificty = \frac{TN}{(FP + TN)}$$
(eq. 5.3)

More information on these performance evaluation measures can be found in [9]. Finally, the accuracy output is considered as the main output, more important than the other ones. For this study to measure the classification performance between normal and abnormal breast tissue and it is calculated as follows:

$$Accuracy = \frac{cases\ with\ true\ negative + cases\ with\ true\ positive}{all\ cases}$$
(eq. 5.4)

After the SVM algorithm had been applied to several initial data samples from different wavelets features and levels, three sets of features were selected to evaluate the performance of SVM over these features. The first set contains the largest 100 approximation coefficients gathered from the wavelet decomposition applied, the second set is the reduced number of coefficients from the first set which contain 10 coefficients generated by the mRMR technique and the final set contains the largest 80 coefficients implemented to investigate the effect on the classification performance results of lowering the number of coefficients without carrying out optimisation.

The following sub sections investigate different issues to find the best classification accuracy that this experiment could achieve based on images of regions of interest. This

includes investigating: different wavelets transform types and number of coefficients, SVM ANOVA kernel parameters tuning and different ROI image sizes.

5.3.3.1 First Series of SVM Experiments

Results from the first series of experiment presented in figures 5.3 to 5.5 show the classification accuracies for three different wavelet transforms using the largest 100 features and the ROI size of 32×32 with degree set to 2 and gamma varying from 1 to 10. By inspecting these figures it appears that the DB2 wavelet of level 1 performs slightly better than the Haar wavelet of level 1 reaching an accuracy of 93.9% when the SVM is tuned to degree value 3, while DB4 level 2 is much lower than Haar and DB2.
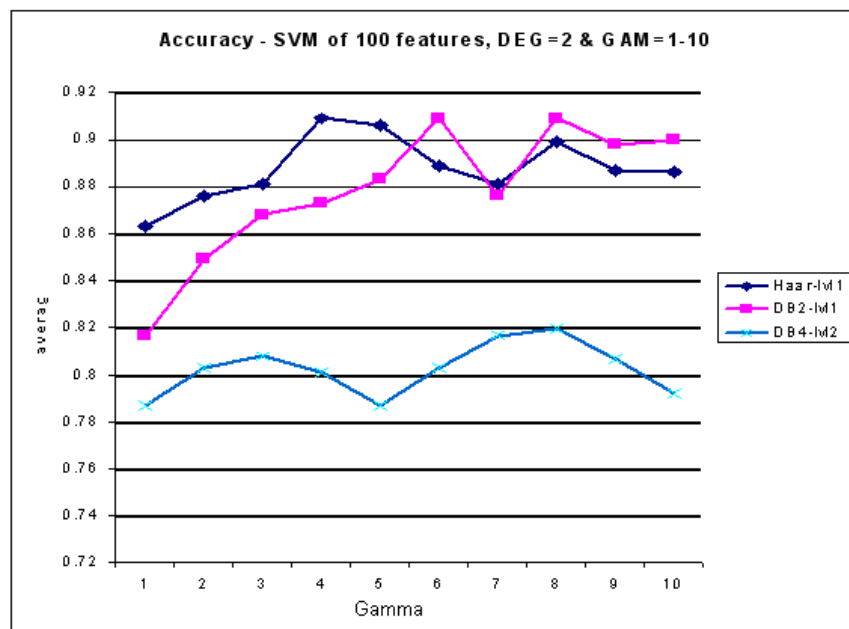
Figure 5.3 Accuracy results using100 features with degree parameter = 2, applied on 3 wavelet transforms: Haar level1, Db2 level1 and Db4 level2
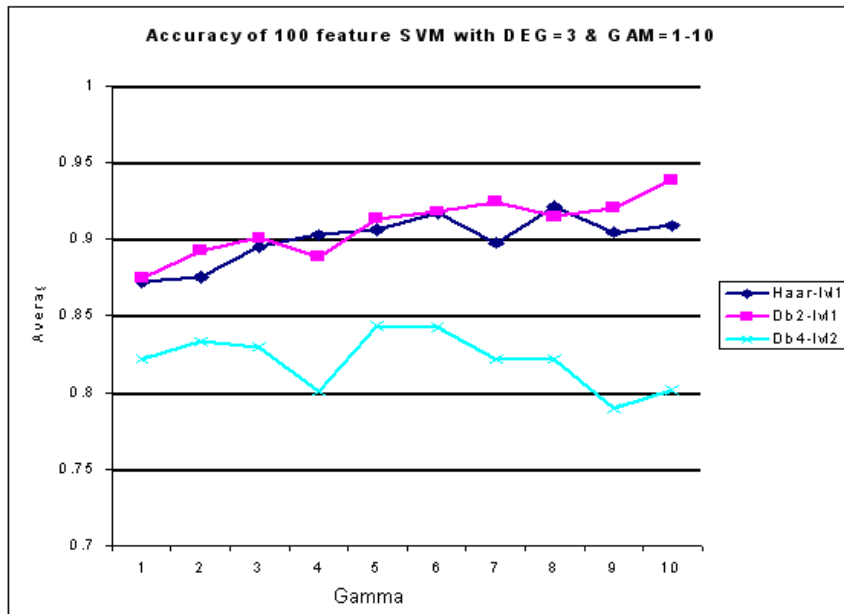
Figure 5.4 Accuracy results using 100 features with degree parameter = 3, applied on 3 wavelet

transforms: Haar level1, Db2 level1 and Db4 level2
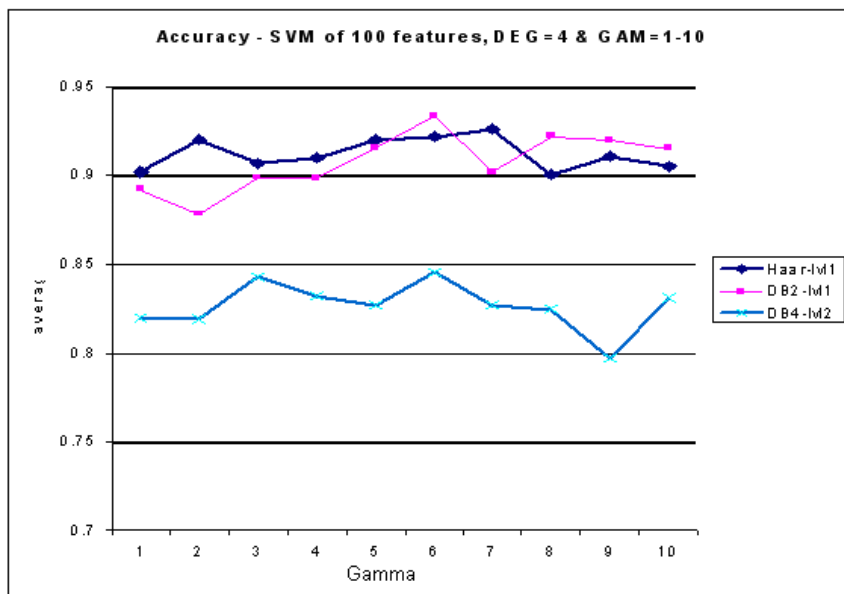
Figure 5.5 Accuracy results using 100 features with degree parameter = 4, applied on 3 wavelet

transforms: Haar level1, Db2 level1 and Db4 level2

Figures 5.6 to 5.8 present graphs showing the classification accuracies using 10 features, extracted by the mRMR from the largest 100 wavelet features, using Haar, DB2 and DB4 level 1 and level 2 decomposition. In these results the DB2 wavelets of level 1 and 2 perform better than other wavelet features shown. However, DB2 level 2 performs slightly better than DB2 level 1 achieving an accuracy of 90.6%.
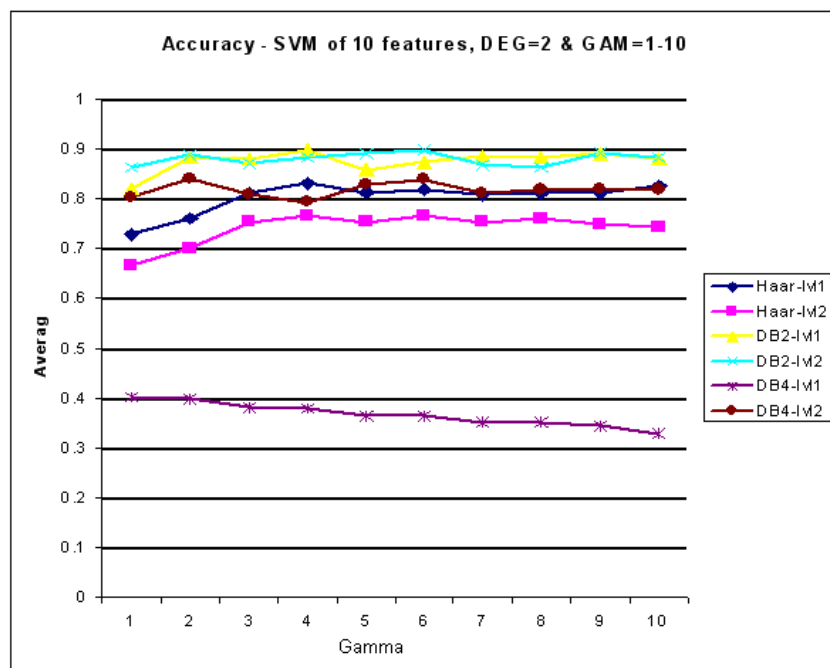
Figure 5.6 Accuracy results using 10 features with degree=2 for several wavelet transforms
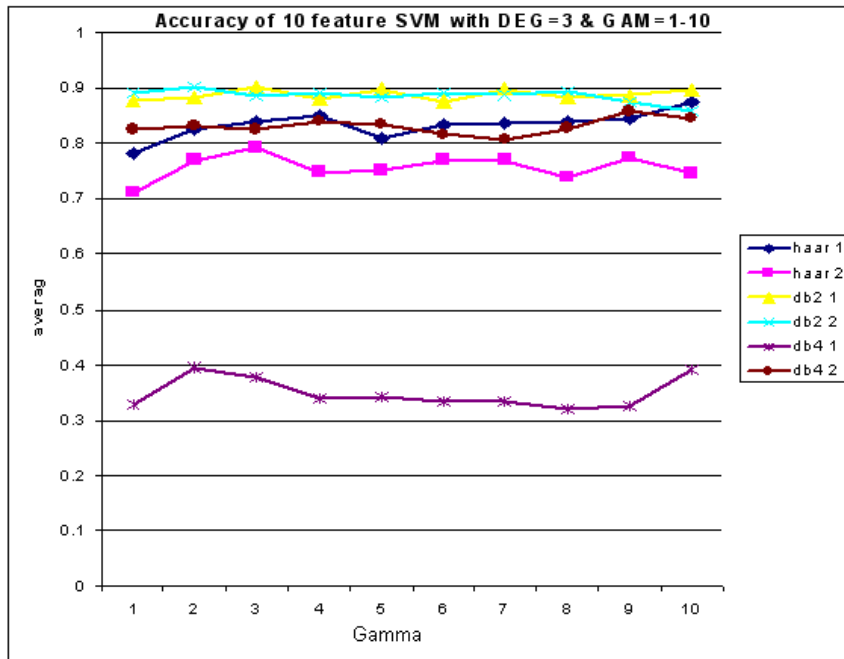
Figure 5.7 Accuracy results using 10 features with degree=3 for several wavelet transforms
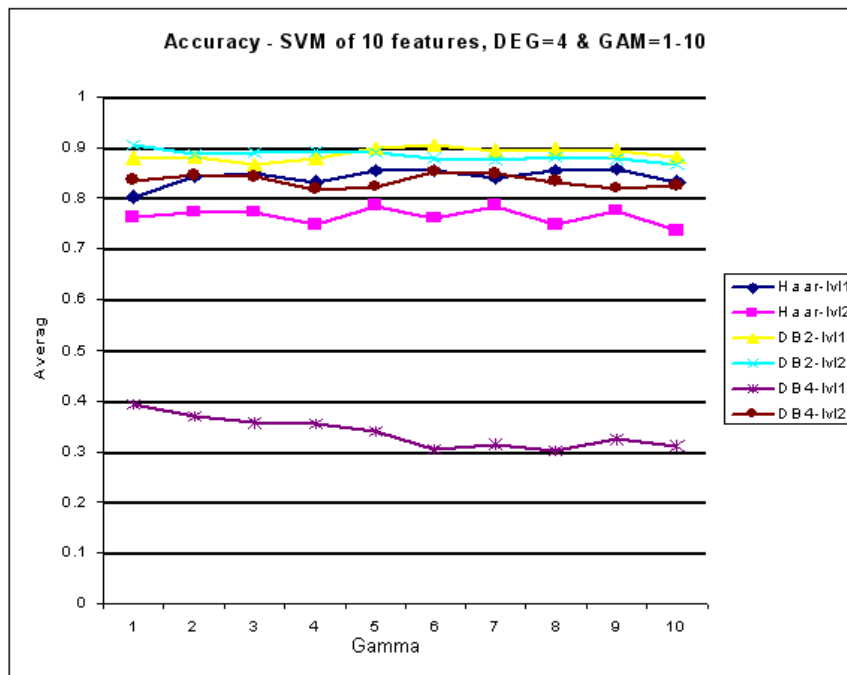
Figure 5.8 Accuracy results using 10 features with degree=4 for several wavelet transforms

Further tests were carried out using the main wavelet transforms (i.e. Haar and Daubechies wavelets with decomposition level 1) using the largest 80 features to investigate the variation of classification performance with different numbers of features. Table 5.1 and Figure 5.9 compare the results obtained for 80 and 100 features for the SVM parameter Degree set to 2, 3, 4 and 5 on individual tests. It is clear that Degree value 5 is not as effective as the other values. However, it appears that the Daubechies wavelet of order two and level 1 using the largest 100 features performed better than the others reaching 93.9% classification accuracy.

Table 5.1 Accuracy results from applying different number of features

	Deg 2	Deg 3	Deg 4	Deg 5
DB2 (80) level 1	91.60%	92.20%	91.60%	80%
DB2 (100) level 1	89.70%	93.90%	93.70%	34.30%
Haar (80) level 1	91.10%	91.70%	91.50%	78.70%
Haar (100) level 1	90.90%	92.20%	92.60%	51.10%
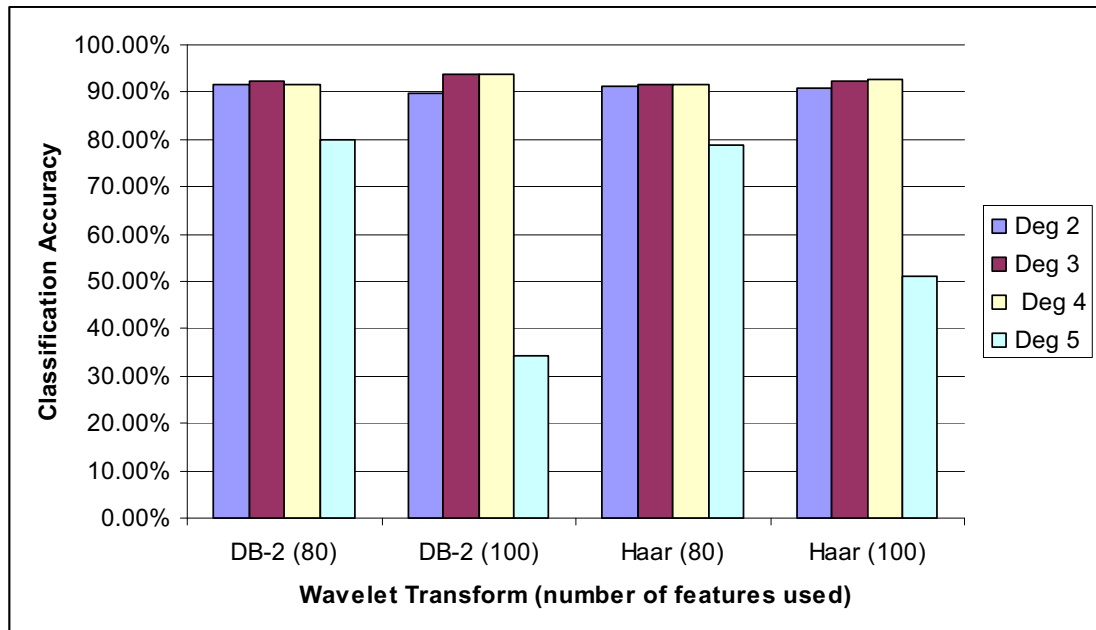
Figure 5.9 Comparing the SVM classification accuracy between the largest 100 features and the largest 80

features of DB-2 and Haar wavelets from level 1 decomposition

5.3.3.2 Second Series of SVM Experiments

In this second series of experiments, more wavelet Transforms were applied to further investigate the difference in performances between wavelet types. Moreover, three datasets were used in these experiments the first containing ROI images of size 32×32 pixels from the large size images of the MIAS database while the second dataset contains images with the following sizes 128×128 pixels, 256×256 pixels, 512×512 pixels and 1024×1024 pixels also from the large size images of the MIAS database. The third dataset included in these experiments contains ROI images from the Mini-MIAS database with a ROI size of 64×64 pixels.

This series of experiments include the wavelet transforms Biorthogonal 2.6 level 2, Biorthogonal 3.3 level 1 and level 2, Discrete approximation of Meyer level 2, Symlets 6 level 2 as well as the wavelet types that applied earlier, Haar level 1 and level 2 and Daubechies 2 level 1 and level 2.

Starting with the second dataset, that contains a variety of ROI sizes that represent clusters of microcalcifications, SVM parameters exponential degree and gamma were tuned for each wavelet features several times to investigate the possibilities of combining wavelet transforms with support vector machines. Therefore, the exponential degree was changed manually from 2 to 10 and for each value the gamma parameter was altered automatically from 1 to 10. Looking at the classification accuracies presented in Figure 5.10, it appears that the SVM parameter, exponential degree, when tuned to 2, 3 or 4 achieved a higher accuracy than the rest.
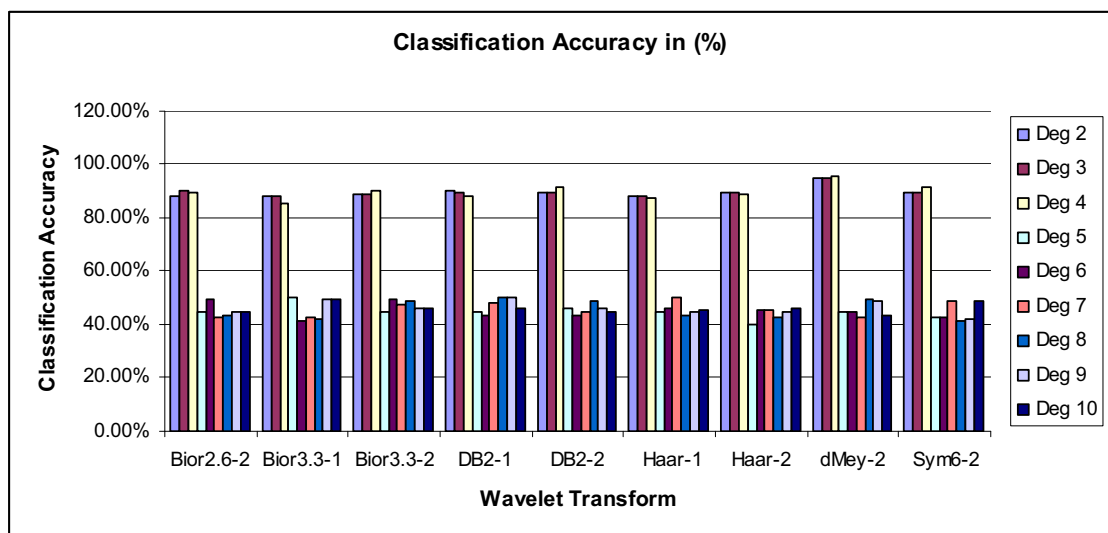
Figure 5.10 SVM classification of different wavelet decomposition features represented in percentage

Table 5.2 shows the variations in performance in these experiments more clearly and Figure 5.11 is a close-up diagram from Figure 5.10 focusing on exponential degree 2, 3 and 4 only as these values achieved the highest accuracy results. The results show that the parameter exponential degree when tuned to 2, 3 or 4 produces acceptable results for tissue classification accuracy reaching 95.3% with dMey wavelet on level 2 of decomposition and exponential degree = 4.

Table 5.2 Classification performance of best output values from this experiment

	Bior2.6 level 2	Bior3.3 level 1	Bior3.3 level 2
Deg 2	88.00%	88%	89%
Deg 3	90%	88%	88.94%
Deg 4	89.30%	85.30%	90.00%
Deg 5	44.70%	50%	44.70%
Deg 6	49.30%	41.30%	49.30%
Deg 7	42.70%	42.70%	47.30%
Deg 8	43.30%	42%	48.70%
Deg 9	44.70%	49.30%	46%
Deg 10	44.70%	49.30%	46%
	dMey level 2	**DB2 level 1**	**DB2 level 2**
Deg 2	95%	90.00%	89.32%
Deg 3	94.70%	89.30%	90%
Deg 4	95.30%	88%	91.30%
Deg 5	44.70%	44.70%	46%
Deg 6	44.70%	43.30%	43.30%
Deg 7	42.70%	48%	44.70%
Deg 8	49.30%	50%	48.70%
Deg 9	49%	50%	46%
Deg 10	43%	46%	44.70%
	Sym6 level 2	**Haar level 1**	**Haar level 2**
Deg 2	89.30%	88%	89.30%
Deg 3	89%	88%	89.36%
Deg 4	91.30%	87.30%	88.70%
Deg 5	42.70%	44.70%	40%
Deg 6	42.70%	46%	45.30%
Deg 7	48.70%	50%	45.30%
Deg 8	41.30%	43.30%	42.70%
Deg 9	42%	44.70%	44.70%
Deg 10	48.70%	45.30%	46%
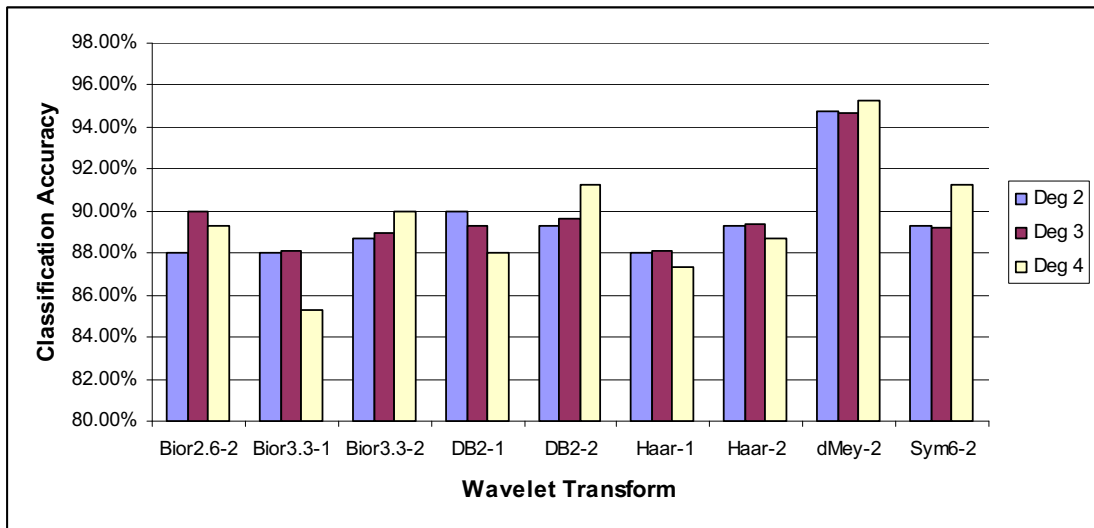
Figure 5.11 Close view on the highest classification accuracy using Exponential Degree values 2, 3 and 4

Furthermore, the classification process has been also carried out on cropped segmented 8-bit grey scale ROI images that represent clusters of microcalcifications. This classification test performed slightly better on the 8-bit ROI images than binary images. The following table illustrates the classification accuracy percentage followed by a graph to represent the accuracy visually. The classification accuracy result from this test was 96% using the dMey wavelet from decomposition of level two between regions of normal breast tissue and regions with microcalcification abnormality.

Table 5.3 Classification accuracy percentage using 8-bit ROI images

	Haar level 2	db2 level 2	bior33 level 2	Sym6 level 2	dMey level 2
Deg 2	0.92	0.947	0.907	0.94	0.96
Deg 3	0.933	0.927	0.887	0.92	0.947
Deg 4	0.913	0.927	0.907	0.927	0.953
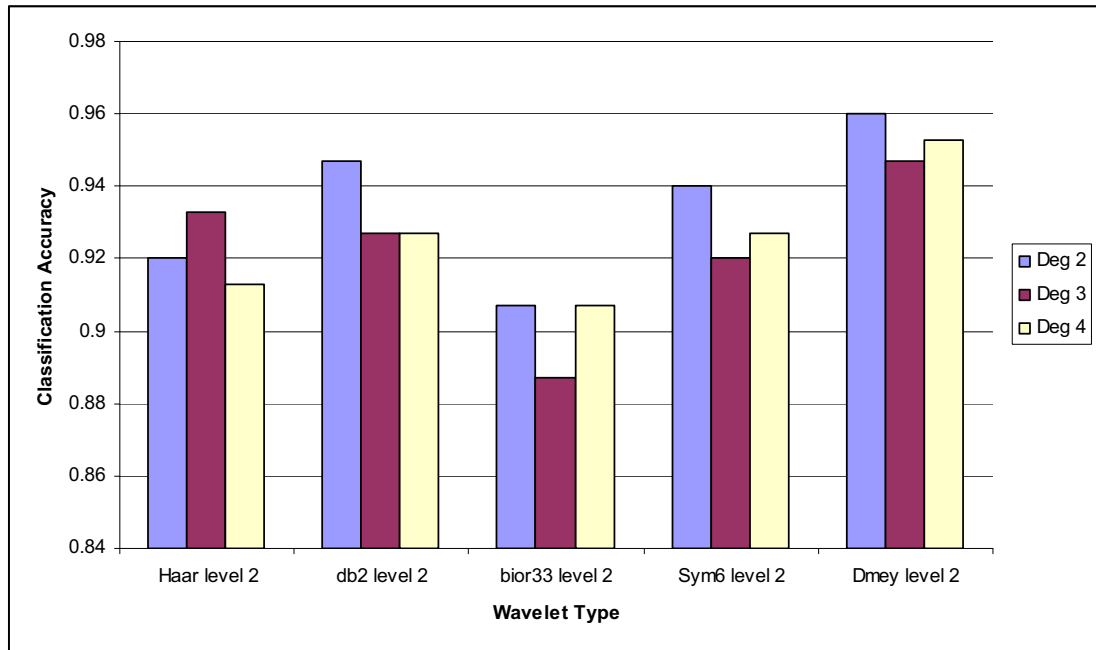
Figure 5.12 Classification accuracy performance using 8-bit ROI images from different wavelet types

The same series of experiments were conducted on the first dataset containing ROI images of size of 32 × 32 pixels that represent an individual microcalcification in each ROI image. All the wavelet transforms applied were from level two decomposition and included Haar, Daubechies DB order 2, Bior order 2.6, Bior order 3.3, Sym order 6 and dMey wavelets. The classification accuracy results are presented in Table 5.3 and Figure 5.12 showing the exponential degree tuned to 2, 3 and 4 producing slightly higher results than the previous test achieving 96.8% of accuracy.

Table 5.4 Actual classification accuracy of 32 × 32 ROI images

	dMey	Sym6	Haar	DB2	bior2.6	bior3.3
Deg 2	79.40%	91%	96.80%	89.30%	95.30%	95.20%
Deg 3	73.20%	83.90%	91.50%	86.10%	87.60%	88.90%
Deg 4	76.60%	86.40%	92.30%	87.50%	95.20%	94.90%
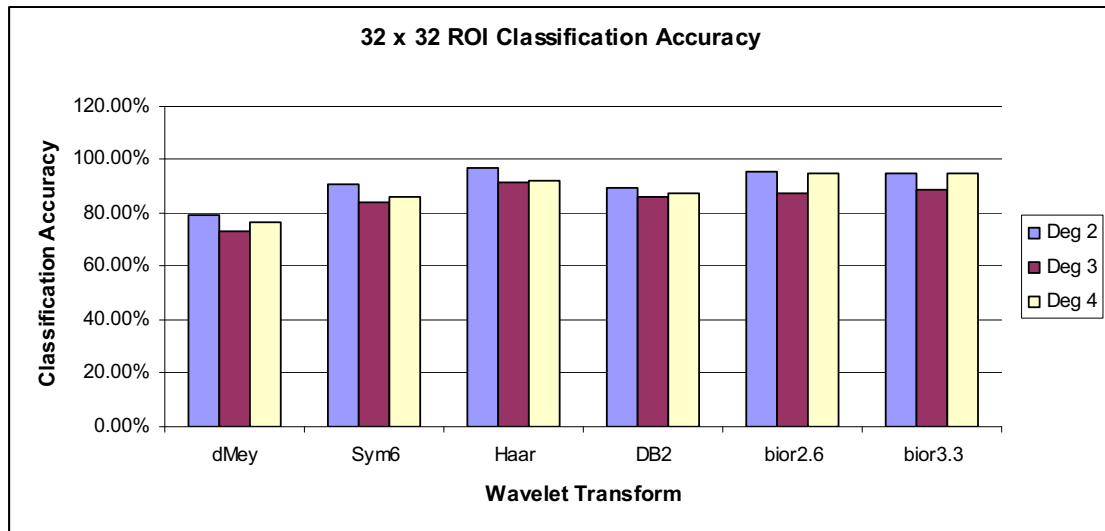
Figure 5.13 ROI 32 × 32 classification accuracy

The series of experiments were also conducted on the third dataset containing ROI images of size 64 × 64 pixels, but this time from the mini-MIAS database. The results of the classification accuracy are presented in Table 5.4. This experiment applied six different wavelet types on clusters of microcalcifications ROI images from the mini-MIAS database. This was to investigate if the procedures applied on the ROI images extracted from the original MIAS database could be successfully applied on the mini-MIAS as well.

Table 5.5 Actual classification accuracy of 64 × 64 ROI images

	Haar level 1	DB2 level 1	Bior1.1 level 1
Deg 2	0.8	0.793	0.767
Deg 3	0.78	0.8	0.807
Deg 4	0.753	0.767	0.78
	Coif level 1	Sym level 1	dMey level1
Deg 2	0.793	0.78	0.727
Deg 3	0.82	0.8	0.767
Deg 4	0.793	0.8	0.727

The results achieved in these experiments enables comparisons to be made with other studies on the same images using different methods as presented in Table 5.5. This comparison is based on comparing the methods that have been applied, the sizes of the images that have been used, from which database images are obtained and finally comparing the average classification accuracy (ACC), based on cropped ROI images, achieved between normal and abnormal tissue region.

Table 5.6 Comparisons with other studies

Algorithm	ACC (%)	Methods	Image size and origin
Rafayah *et al.* [10]	87.5%	DB4 wavelet & fuzzy neural	800 × 800 ROI, from MiniMIAS
Sheshadri and Kamdaswamy [11]	75%	using optimal filter and statistical texture features	256 × 256 ROI and full image from MiniMIAS
Ferreira and Borges [12]	83.3% 88.8%	Haar wavelet, DB4 wavelet with Euclidian distance	64 × 64 ROI, from MiniMIAS
Proposed system with ROI set 2 (Binary and 8-bit)	95.3% for Binary ROI 96% for 8-bit ROI	dMey wavelet level 2 with SVM	128 × 128, 256 × 256, 512 × 512 and 1024 × 1024 ROIs from Large MIAS
Proposed system with ROI set 1	96.8%	Haar wavelet level 1 with SVM	32 × 32 ROI, from Large MIAS
Proposed system with ROI set 3	82%	Coiflets wavelet level 1 with SVM	64 × 64 ROI, from mini-MIAS

5.4. Summary:

This chapter presents the experiments that have been completed to choose a machine learning technique that could handle the wavelet features as an input, and also manage the classification output as supervised technique for two output classes. Two different types of machine learning, the radial basis function (RBF) and support vector machines (SVM) were tried, but the SVM performed much better than the RBF. This is perhaps not surprising, since the SVM is said to be guaranteed to converge to a global minimum during training and to have better generalisation capabilities than neural networks [2]. Furthermore, it is an excellent tool for binary classification problems by seeking the optimal separating hyperplane. This provides efficient separation for the data and maximises the margin. However, combining feature extraction method with a machine learning technique in an optimum manner is a difficult process which takes significant time to achieve.

Although there is more to investigate in the area of machine learning especially SVM, the current work has shown that it can handle the classification of microcalcification data. The results that have been achieved combining SVM and wavelet decomposition, with a classification accuracy reaching 96.8%, are comparable to some of the best in the field of mammography and are considered very satisfactory.

References

1. Sewell, M. *Support Vector Machines (SVMs)*. [cited 2009 February]; Available from: http://www.svms.org.

2. Qahwaji, R. and Colak, T., *Automatic Short-Term Solar Flare Predection Using Machine Learning and Sunspot Associations.* Solar Physics, 2007. **241**(1): pp. 195-211.

3. Vapnik, V., *The Nature of Statistical Learning Theory*. Springer Verlag. 1999, New York.

4. Qu, M., Shih, F.Y., Jing, J., and Wang, H., *Automatic Solar Flare Detection Using MLP, RBF, and SVM.* Solar Physics, 2003. **217**(1): pp. 157-172.

5. Sutton, R.S. and Barto, A.G., *Reinforcement Learning: An Introduction*. 1998: MIT Press.

6. Bishop, C.M., *Neural Networks for Pattern Recognition*. 1995, London: Oxford University Press.

7. Fukunaga, K., *Introduction to statistical pattern recognition (2nd ed.)*. 1990: Academic Press Professional, Inc. 592.

8. Colak, T. and Qahwaji, R., *Automated Prediction of Solar Flares Using Neural Networks and Sunspots Associations.* Advances in Soft Computing, 2007. **39**: pp. 316-324.

9. Fawcett, T., *An introduction to ROC analysis.* Pattern Recognition Letters, 2006. **27**(8): pp. 861-874.

10. Rafayah, M., Qutaishat, M., and Abdallah, M., *Breast cancer diagnosis system based on wavelet analysis and fuzzy-neural.* Expert Systems with Applications, 2005. **28**(4): pp. 713-723.

11. Sheshadri, H.S. and Kandaswamy, A., *Computer Aided Diagnosis of Digital Mammograms.* Information Technology Journal, 2006. **5**(2): pp. 342-346.

12. Ferreira, C.B.R. and Borges, D.L., *Analysis of mammogram classification using a wavelet transform decomposition.* Pattern Recognition Letters, 2003. **24**(7): pp. 973-982.

Chapter 6

Conclusion and Future Work

6.1. Thesis Conclusion

This thesis presents recent work towards the design of systems for the automated diagnosis of breast cancer by analyzing digital mammogram images to provide radiologists with a second opinion. The work presented in this thesis provides a contribution to existing systems dealing with digital mammogram images by combining discrete wavelet transform (DWT) and support vector machines (SVM) with the ANOVA kernel in way that has not been done before. This work done using the MIAS database, demonstrates that automated diagnosis of digital mammograms can be done using computationally simple methods and algorithms and achieve results with high accuracy for the classification between cropped regions of interest of normal and abnormal breast tissue.

There are three main stages in this study and each stage has been implemented several times to ensure that the experiments have been properly performed and, where necessary, to tune algorithm parameters or function types to give the best results. These stages are: (1) separate the background from the foreground that contains suspicious objects from within cropped regions of interest; (2) feature extraction to represent the characteristics of segmented objects in a compact form; (3) classification of regions of interest containing suspicious objects, based on the extracted features, into two classes. These stages have been described in Chapters 3, 4 and 5 respectively.

Chapter 3, where the presentation of the practical work starts, focuses on regions of interest extracted from whole image. These regions of interest are cropped manually based on locations highlighted from the MIAS manual; this has to do with the point of view that radiologists can be selecting the region of interest rather than letting the system do it automatically. Alternatively, letting the trained system analyse whole images will take a little longer. After that, all the regions of interest (ROI) images are segmented keeping only suspicious objects. The segmentation process will generate new ROI images in two forms; the first is segmented binary ROI images and the second is segmented ROI 8-bit images. Chapter 4 describes the implementations of the feature extraction method and its organisation for the next stage. Finally, Chapter 5 presents the classification method used to separate ROI image features into either normal region or abnormal region classes.

The MIAS database has been very useful for this study as it provides a variety of cases. There are 25 cases of mammogram images that include microcalcifications. These images have been cropped to create a new dataset containing ROI images of size 32×32 pixels. This size is used mainly to represent individual microcalcifications in one image. Another dataset has been created that contains ROI images with larger size than the previous one to include clusters of microcalcifications and these sizes are: 128×128, 256×256, 512×512 and 1024×1024 pixels. Finally, a third dataset has been also created, this time from the Mini-MIAS database with a size of 64×64 pixels, which also includes clusters of microcalcifications. During the segmentation process an evaluation between the square filter shape and circular shape has been produced to find that the percentage of detecting suspicious objects within a region of interest using a circular filter shape is 0.0157% of the image which is higher than the square filter shape of 0.0102%

using the threshold value of 10. The procedure of the segmentation is to help the system locate microcalcifications or suspicious objects within ROI images for further analysis. Since all ROI images may contain abnormalities within an image a classification method is needed to be able to distinguish between normal ROI images and ROI images that contain microcalcifications.

The general performance of the system has produced acceptable results in terms of measured classification accuracy. The results were evaluated using different sizes of regions of interest with results as follows: with the ROI images representing individual microcalcification, the accuracy of classification into normal and abnormal cases was 96.8 %; with the ROI images that represent cluster of microcalcification the accuracy of classification was 95.3 % for segmented binary ROI images and 96% for segmented 8-bit ROI images; with the ROI images from the mini-MIAS database including clusters of microcalcifications the accuracy of classification was 82%.

6.2.   Thesis Contribution

The contributions in this thesis can be summarized as follows:

- The thresholding technique to detect masses by Kom *et al.* in [1] was modified so that to be able to detect microcalcifications, which are considerably smaller abnormalities than masses. This technique assists this study to detect microcalcifications, by removing the background surrounding the microcalcification, without the need to apply more complex pre-processing steps such as image enhancement. The filter was able to locate microcalcifications in different ROI images either the ones that represent a cluster of microcalcifications or images that represent individual

microcalcification from datasets that contain normal and abnormal ROI images.

- Using the discrete wavelet transform approximation coefficients to extract features from the segmented images (i.e. black and white images and 8-bit images) proved to be a powerful tool to extract unique features from the dataset of ROI images.

- Combining the support vector machine, using the ANOVA kernel, with the discrete wavelet transform, using approximation coefficients, produced some good classification results in this application. To the best of my knowledge this type of SVM has not been applied before in the mammography area. Additionally, in this study the SVM was found to perform better than radial basis function NNs when combined with wavelet transform. This has been found also in other areas of research [2-6].

- Regions of interest can include different types of information and therefore in this study various ROI images have been studied including normal and abnormal breast tissue. The ROI images have been divided into two sets, the first set represents individual microcalcification with a size of 32×32. The second set represents cluster of microcalcifications with different sizes depends on how big the cluster is, and they are: 128×128, 256×256, 512×512 and 1024×1024. It was found that using the same techniques of segmentation, feature extraction and classification on all ROI sizes mentioned in this study achieved acceptable results with only slight difference. It was not found necessary to use different methods to study individual or clusters of microcalcifications.

6.3. Suggestions for Future Work

Although the work in this study reached its main objectives by achieving high classification accuracy between normal and abnormal breast tissue, it has also shown the need for further investigations to be carried out in particular aspects.

- At the segmentation stage, the thresholding filters were fixed with radii of 1.5 pixels for peaks and 11 pixels for the surrounding region in order to detect microcalcifications, bearing in mind that the size of individual microcalcification is between 0.1 mm and 1.0 mm. Use with different image resolutions could mislead the detection process. Therefore, developing filters that dynamically adapt to the image resolution would improve the versatility of the process. In principle the same approach could be applied to the detection of the mass type of abnormality. However, masses should definitely be processed with different filter sizes as masses, at between 3mm and 50mm in size, are much larger than microcalcifications as mentioned in Chapter 2. Furthermore, such research would need a radiologist to be involved to check on the process of detection and classification.

- The feature extraction stage was implemented using discrete wavelet transforms by extracting wavelet coefficients and considering only the 100 largest coefficients, as the DWT produces a large number of coefficients. Although several wavelet types have been considered within this study, there are many more wavelet types that could be investigated as well as the appropriate level of decomposition to be applied. It is interesting to compare different wavelet decompositions from different levels as each wavelet has its own characteristics. Furthermore, there are other features that could be

extracted from wavelet decompositions that may be useful for different types of abnormalities. This could lead to many different studies.

- The support vector machine has been tested in this work using the ANOVA kernel and produced satisfactory results when combined with the DWT. Although the SVM has been compared with and found to outperform NNs using radial basis function, there are other neural networks types and structures that could also be investigated.

- Several mammography databases are available for researchers to study, as mentioned in Chapter 2; there are the DDSM, Nijmegen and LLNL. Even though this would take considerable effort it could be useful to train a system on one database and test it on another. This could increase the efficiency of the system to detect a variety of abnormalities and test different densities of breast tissue, even though there is no similarity between them.

- Finally, reconstructing 3-dimensional images from 2-dimensional images could improve the diagnosis by making it easier to locate a tumour in the breast and identify the size and depth of the abnormality. This could be obtained from default views taking mammograms vertically and horizontally.

References:

1. Kom, G., Tiedeu, A., and Tiedeu, M., *Automated detection of masses in mammograms by local adaptive thresholding.* Computers in Biology and Medicine, 2007. **37**(1): pp. 37-48.

2. Distante, C., Ancona, N., and Siciliano, P., *Support vector machines for olfactory signals recognition.* Sensors and Actuators B: Chemical, 2003. **88**(1): pp. 30-39.

3. Huang, Z., Chen, H., Hsu, C.J., Chen, W.H., and Wu, S., *Credit rating analysis with support vector machines and neural networks: a market comparative study.* Decision Support Systems, 2004. **37**(4): pp. 543-558.

4. Mahesh, P. and Mather, P.M., *Assessment of the effectiveness of support vector machines for hyperspectral data.* Future Generation Computer Systems, 2004. **20**(7): pp. 1215-1225.

5. Nurettin, A. and Cüneyt, G., *Automatic recognition of sleep spindles in EEG by using artificial neural networks.* Expert Systems with Applications, 2004. **27**(3): pp. 451-458.

6. Qu, M., Shih, F.Y., Jing, J., and Wang, H., *Automatic Solar Flare Detection Using MLP, RBF, and SVM.* Solar Physics, 2003. **217**(1): pp. 157-172.

Appendix 1

List of Publications

Conference:

1. Osta, H., Qahwaji, R., and Ipson, S., "*Comparisons of feature selection methods using discrete wavelet transforms and Support Vector Machines for mammogram images*", The 5th International Multi-Conference on IEEE Systems, Signals and Devices (SDD), 2008, pp. 1-6, Amman, Jordan

2. Osta, H., Qahwaji, R., and Ipson S., "Wavelet-based Feature Extraction and Classification for Mammogram Images using RBF and SVM", Visualization, Imaging, and Image Processing (VIIP) 2008, Palma de Mallorca, Spain

Journal:

1. AbuBaker, A. A., Qahwaji, R.S., Aqel, M. J., Al-Osta, H., Saleh, M. H., "Efficient Preprocessing of USF and MIAS Mammogram Images," Journal of Computer Science, Vol. 3, No. 2, pp. 67-75, 2006